2006 Svalbard Experimental Spill to Study Spill Detection and Oil Behavior in Ice

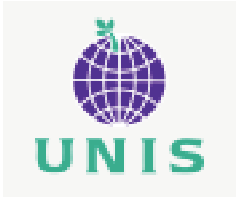

2006 Svalbard Experimental Spill to Study Spill Detection and Oil Behavior in Ice

Final Technical Report

December 15, 2006

United States Department of Interior
Minerals Management Service
Contract Number 1435-0106-CT-3925

Submitted by:

DF Dickins Associates Ltd.
David Dickins
info@dfdickins.com

SINTEF
Per Johan Brandvik
per.brandvik@sintef.no

The University Center in Svalbard (UNIS)
Liv-Guri Faksness
liv-guri.faksness@unis.no

Boise State University
John Bradford and Lee Liberty
johnb@cgiss.boisestate.edu

ACKNOWLEDGEMENTS

The authors wish to acknowledge the support of the following funding agencies and their representatives who made this project possible.

Funding Partners

Organization	Technical Representative(s)
Minerals Management Service	Joseph Mullin
Alaska Department of Environmental Conservation	Dianne Munson
STATOIL ASA	Arne Myhrvold Hanne Grieff Johnsen
Shell Technology Norway	Knut Bakke and Gina Ytterborg
ConocoPhillips	Ian Denness
ExxonMobil	Jim Clarke
Alaska Clean Seas	Lee Majors
Store Norske Spitsbergen Kullkompani	Harry Vinje and Per Nilsen

This study was funded by the Minerals Management Service, U.S. Department of the Interior, Washington, D.C. under Contract Number 1435-01-06-CT-39295.

The project team would also like to thank Store Norske Kull Kompani for their cooperation and flexibility in allowing personnel and supplies to be transported onboard their charter aircraft during a busy period at the Svea mine.

OVERALL PROJECT ORGANIZATION

DF Dickins Associates Ltd. and SINTEF jointly managed the project according to the following contractual arrangements:

- **Remote Sensing**: Boise State University and Exploration Technologies contracted through DF Dickins, funded by the Minerals Management Service (MMS), Alaska Department of Environmental Conservation (ADEC), Conoco Phillips, ExxonMobil and Alaska Clean Seas (ACS)

- **Oil Behavior and Fate and Countermeasures Evaluation**: UNIS contracted through SINTEF and SINTEF contracted directly to STATOIL, Shell Technology Norway and Store Norske Spitsbergen Kullkompani (remainder subcontracted through DF Dickins under MMS contract – see above)

DISSEMINATION AND APPLICATION OF RESULTS

Findings from this project are publicly available. The full report will be posted on the MMS website www.mms.gov/taroilspills/ early in 2007. The authors plan to produce a manuscript for peer-reviewed Journal publication with key findings. Preliminary presentations and papers already prepared and presented on specific aspects of the program include Brandvik et al. (2006) and Liberty et al. (2006). Several ongoing and planned research programs are expected to benefit from this study:

- Oil Spill Contingency for Arctic and Ice-infested Waters – JIP (Joint Industry Program) administered by SINTEF, 2006-2009.
- Detection of Oil on and Under Ice – Phase III: Evaluation of Higher-Powered Airborne Radar Systems to Detect Oil Under Ice. Contract in processing for 2006/07 funding by MMS. Contractors: DF Dickins Associates Ltd. and Boise State University.

DISCLAIMER

This report has been reviewed by the Minerals Management Service and approved for publication. Approval does not signify that the contents necessarily reflect the views and policies of the Service, nor does mention of trade names or commercial products constitute endorsement for use.

SUMMARY, CONCLUSIONS AND RECOMMENDATIONS

This project encompassed three research areas related to improving the level of understanding of and response to accidental spills in ice:

1. Remote sensing: detection and mapping of oil under ice;
2. Oil in ice, fate and behavior; and
3. In-situ burning evaluation.

The experiment was designed around the concept of a controlled oil release under ice with sufficient surface area, volume and film thickness to permit measurements at a realistic field scale. A volume of 3,400 liters of Statfjord crude oil was successfully released on schedule, and fully contained within a skirt inserted through the ice. Divers measured the oil film thickness distribution under the ice using a specially developed probe. Monitoring of the oil under the ice was achieved with a combination of divers and through-the-ice video cameras. The spill was effectively removed through in-situ burning on the ice. The following summary highlights key results, conclusions and recommendations within each of the three research areas.

Remote Sensing

Ground Penetrating Radar: Surface-based ground-penetrating radar (GPR) operating at 500 MHz clearly delineated changes at the ice water interface caused by emplacement of oil. Further, this experiment demonstrated that GPR operated from the ice surface is capable of differentiating oiled regions of the ice under surface from the background response. Based on a qualitative comparison of the measured oil thickness distribution and radar results, it appears that the lower detection limit at a frequency 500 MHz is on the order of 1 to 3 cm oil film thickness.

The airborne radar tests were not as definitive, however it does appear that the 500 MHz system is capable of penetrating at least 0.65 m of relatively warm sea ice and the potential to detect oil from an airborne platform with higher-power radar systems in the future looks promising. At a frequency of 1000 MHz, it is possible to image the snow pack and snow ice interface in detail from a low altitude airborne platform (5 to 10 m), suggesting a strong potential to detect oil at the ice/snow interface with existing off-the-shelf systems. There is a broad application for GPR in this role, as evidenced by a recent decision by Alaska Clean Seas to purchase a dedicated GPR system for detection of future accidental spills under snow originating from above-ground pipelines.

Different radar imaging attributes are sensitive to varying thickness of oil films. A phase change (or change in the reflected wave shape) was observed over most of the containment area after oil was emplaced and may prove to be the most robust indicator of the presence of oil. The phase change was most prevalent in the area of thick oil where reversed polarity was observed. A high amplitude response was observed in areas where the oil film thinned and reflections from the top and base of the ice interfere.

Optimal detection in an uncontrolled setting will require simultaneous computation and analysis of each of these waveform attributes. Software developed under an earlier phase of this project is designed with this capability (Bradford, 2005).

In addition to lateral heterogeneity at the surface and within the ice matrix, complexity at the ice/water interface has a significant impact on the GPR attributes. Deterministic measurement of these variations is exceedingly difficult but would be required to compute oil film thicknesses from the measured GPR response. Therefore, while it is possible to determine whether oil is present or not, it is considered unlikely that meaningful measurements of film thickness can be made under typical field conditions.

Conclusions: Ground Penetrating Radar was successfully deployed from the ice surface to detect and map the presence of oil under 65 cm of ice. In summary the radar results demonstrated that a well-defined, measurable anomaly is induced by the presence of oil films as thin as 1-3 cm under the ice. The surface radar imaging attributes provide a strong indicator where oil is present and can be clearly differentiated from the background response.

Airborne radar shows strong potential to detect oil at the snow/ice interface with existing systems, and to measure ice thickness and detect oil at the ice/water interface with higher-powered systems in the near future.

Since it is expensive and logistically difficult to conduct more than a handful of large-scale field experiments, future development of radar detection systems will depend largely on an intensive computer modeling effort to understand the radar response to a variety of sea ice conditions and oil types and distributions, and to fully define the limitations of the radar method.

All of the experiments to date have been performed on first-year ice with relatively even top and bottom surfaces. Detection of oil under ice through multi-year ice or rafted/ridged first-year ice might be difficult or impossible. While snow cover does not substantially affect radar penetration, the presence of voids and upturned blocks within rough ice is expected to present a major challenge. Limited experience with operating the GPR over simulated ice rubble (Dickins et al., 2005) gave cause for some optimism that GPR may be able to detect the oil under an uneven ice surface. However, results were not definitive in the tank experiment, in part because of interference introduced by the oil containment skirt.

Recommendations

1. Model the expected radar response to different oil in ice scenarios. Ice parameters would include (not limited to): thickness, porosity, salinity, temperature, roughness, voids, consolidated thickness, and crystal orientation. Oil parameters would include specific gravity, degree of emulsification, film thickness.
2. Evaluate the potential to develop and test an operational airborne radar system capable of detecting oil under ice of different composition and thickness (related to parameters defined above).

3. Continue to improve the display interface to reduce the level of training necessary for responders to use GPR in a field setting.

Note: *These recommendations are incorporated as part of an active proposal to MMS (DF Dickins and Boise State University – in process). It is also planned that new findings and developments in this field will be integrated into the ongoing SINTEF JIP remote sensing component (Project No. 5) with opportunities to try next-generation systems in future experimental spills in Canada and Norway over the period 2007-09.*

Acoustics: Acoustic imaging through sea ice is possible under ideal surface ice conditions, as proven through past trials in Canada. The ice surface must be free of trapped air (e.g. snow) and a solid coupling with the ice surface is required. Acoustic coupling was achieved in this project by removing the snow and applying a small amount of seawater directly to the ice surface immediately before soundings were acquired. Once coupled to the ice surface, the acoustics transducer acquired data along the surface in profile at similar speeds to GPR acquisition. Modeled and field acoustic results suggest that adequate impedance contrasts exist to provide a measurable reflection at ice/water, ice/oil, and oil/water interfaces. Acoustic methods may be preferred over GPR where active brine channels are present (excessive radar attenuation) and where the ice surface is free of snow accumulations, for example relatively young sheets early in the winter.

Conclusions: Acoustic imaging shows promise in identifying crude oil beneath sea ice under certain conditions. However, GPR appears to be a more robust tool to image through sea ice under a wider range of circumstances where substantial snow accumulations are common on the ice surface. Acoustic methods may have their place in specialized applications, for example: smooth ice roads and/or thin ice accumulations where high salinities would reduce the probability of detection with radar. Preliminary findings from this phase of the project are contained in Liberty et al. (2006 and 2007).

Recommendations

4. Conduct further acoustic studies with an arrayed transducer system to enhance the potential to image through a rough ice top or bottom surface. Other system improvements over the relatively simple off-the-shelf hardware deployed in this project could include: Multi-offset transducer acquisition to help measure ice velocities and improve estimates of ice and oil thicknesses; and three-component transducer acquisition to help improve estimates of oil locations and quantity, especially where heavier oil concentrations are present.

Hydrocarbon gas sensing: Direct assessment of optical gas sensing technology was not part of the work scope in this project. However, a limited number of samples were collected in an effort to assess the extent and rate of migration of light hydrocarbon components through the ice as a follow-on to the positive results obtained in the 2004 tank tests with Shell Global's LightTouch™ prototype system (Dickins, et al. 2005). Results of the limited 2006 sample analysis for ethane and other components in the ice are reported in Appendix E. The evaluation was limited in scope by the lack of any ability to safely extract deep cores within the test area following the spill. Coring in this manner would have posed an unacceptable risk of allowing trapped oil to surface prematurely and jeopardizing the oil behavior studies.

There was evidence of elevated levels of key components within ten's of centimeters above visible oil in a number of the ice cores but it is still not clear that sufficient flux levels of ethane or other marker gases will be present on the surface within a reasonable time following a spill under ice for remote ethane sensors to be used as a reliable detection tool.

Conclusions: Optical gas sensing showed promise through measurements made during the original 2004 tank studies. The latest generation of sensors have an order of magnitude more sensitivity than the prototype available for the initial trials (W. Hirst, pers. comm). In addition the size and weight of the system has shrunk dramatically to the point that the current instrument can be flown in a relatively small aircraft. Regardless of questions remaining as to whether ethane sensing is a useful tool for oil under ice detection, this technology appears to have great potential to detect oil on the surface under snow and/or mixed with slush and brash ice between floes in all weather conditions.

Recommendations

5. Deploy the latest generation LightTouch™system incorporating lightweight, portable methane and ethane sensors in experimental spills being planned through the ongoing SINTEF Joint Industry Program (2006-09) and other agencies. Future evaluations of this technology should focus on a variety of oil in ice scenarios, rather than being limited solely to the application of detecting oil under ice.

Oil Behavior and Countermeasures

The weathering of the oil under the ice with respect to vertical migration, evaporative loss and water content was monitored through oil and ice sampling at regular intervals throughout the field period. The oil was first observed on the surface after 24 days under the ice (March 27 to April 20). Water content of the surface oil in the melt pool was, as expected, very low (0-8 vol.%), and the final evaporative loss was measured at 27% on May 30 (63 days after the spill).

The water-soluble components in the ice cores sampled outside the skirted area before and after the oil release had no significant difference in concentration (0.05 to 1.09 ppb sum Water Accommodated Fraction (WAF)). The shallow cores taken inside the skirted area after the oil release showed also no significant difference in concentration of water-soluble components (0.01 to 0.1 ppb sum WAF). However, the reference cores showed increased content of water-soluble components after 24 days, attributed to migration of these components in the porous first-year ice (no bulk oil was present in these cores). By that time, the oil had migrated through the ice and was present in the snow inside the skirted area (April 20). Later sampling of reference cores (May 10, 20 and 29) showed the presence of bulk oil components due to spreading of bulk oil through the surface snow/slush/water layer.

In-situ burning of the surface oil was performed with a simple hand held igniter (gelled n-hexane). Flame spreading was successful, and approximately 2,500 liters of weathered oil burned down to a solid residue of 106 liters in only 11 minutes (96% effectiveness) with a burn rate of 3.1 mm/min. Preliminary findings from this phase of the project were presented in Halifax at the third NATO/CCMS workshop on oil spill response (Brandvik et al., 2006).

Conclusions: This experiment confirmed that in-situ burning is an effective tool to greatly reduce the environmental impact of oil spills in ice-covered waters with minimal logistics.

Recommendations

6. Further studies should be performed to determine the release rates of water-soluble components in ice from encapsulated oil spills. Such data is important for further research into modeling of the exposure of water-soluble hydrocarbons to Arctic ice fauna.
7. Further laboratory and field studies should be performed with different oil types to quantify the feasibility and effectiveness of in-situ burning under a variety of environmental and ice conditions. This data should be implemented within established oil weathering models (e.g., SINTEF OWM) to improve the accuracy of predicting windows-of-opportunity for various oil types and spill scenarios.

Note: *The ongoing Joint Industry Project – Oil Spill Contingency for Arctic and Ice Infested Waters (SINTEF and partners, 2006-2009) contains research components designed to address a number of these recommendations.*

Table of contents page

LIST OF APPENDICES

1. BACKGROUND

This project encompasses three engineering and scientific research components related to improving the level of understanding and response to accidental spills in ice:

1. Remote sensing detection and mapping;
2. Oil in ice, fate and behavior; and
3. In-situ burning evaluation.

Brief background discussions of previous work in these areas are provided below.

1.1 Detection and mapping oil under ice

A concentrated research effort in the 1980's analyzed and tested a variety of technologies to detect oil in or under solid ice, including radar, electromagnetic and acoustics. Dickins (2000) summarizes the state of the art, based on historical results. None of the older research led to a practical operational system that could be used in a field situation. This ongoing gap in capability was identified as a priority research area in terms of advancing Arctic spill response (Dickins, 2004). With the rapidly increasing interest in Arctic oil exploration and development over the next decade, solutions to the problems of oil in ice detection are likely to remain at the forefront of international research agendas.

Under continued Minerals Management Service (MMS) sponsorship, the development of oil and ice detection systems has made significant progress over the past three years through a series of related projects:

1. A test basin experiment in November 2004 demonstrated the potential for off-the-shelf ground penetrating radar (GPR) systems and an ultra-sensitive ethane sensor to detect oil trapped under model sea ice (Dickins et al., 2005). www.mms.gov/tarprojects/517.htm

2. A follow-on study (March to July 2005), focused on further developing the radar technology into a reliable and more "user friendly" spill response tool. Tasks included:
   - Evaluating available hardware solutions for multi-polarization GPR data;
   - Testing at temperatures down to –20°C (Prudhoe Bay, April 2005);
   - Developing improved radar processing software for the oil-in ice-problem (Bradford, 2005); and
   - Developing a preliminary program design to evaluate oil-in-ice detection systems through a large-scale field spill in Norway in 2006 (leading to this study - Dickins (2005)).

1.2 Oil in ice fate and behavior

Extensive research over the past 20 years includes laboratory studies and field experiments aimed at understanding the fate, behavior and weathering processes for oil spilled under arctic conditions. This research was performed both in the US, Canada and Norway. During the seventies and eighties, active oil exploration in Alaska, Canada, the Barents Sea and on Svalbard led to a number of laboratory and field studies. Smaller experimental oil releases including fresh and emulsified crude under solid ice (up to 6 tonnes per spill) were performed in 1974, 1979, 1981 and 1983 (e.g. NORCOR, 1975, Dickins et al., 1981, Comfort *et al.*, 1983). The first experimental spill in broken ice was carried out in 1986 off Cape Breton Island on the Canadian East Coast (SL Ross and DF Dickins, 1987). This was followed in April 1993 by the first large-scale experimental oil spill (26 m^3) under Arctic pack ice conditions performed in the Barents Sea marginal ice zone (MIZ) (Vefsnmo and Johannessen, 1994; Brandvik *et al*., 2004).

These field experiments proved invaluable in understanding weathering processes of oil in a variety of spill scenarios (including a simulated subsea blowout) and environmental conditions (including wind, waves, ice conditions, drift and spreading in the marginal ice zone). These studies showed clearly that different oils have different weathering properties under Arctic conditions at sea. Field observations regarding weathering at low temperatures and in broken ice were also studied in small and meso-scale lab facilities (Singsaas *et al*, 1994). Payne et al. (1991) describes the different aspects of oil weathering in Arctic environments.

Several reports give a good overview of the state of knowledge. Examples include a final report from the Norwegian program "Oil spill contingency in cold and Arctic areas" - ONA I and II (Løset *et al*., 1994) and "Oil spill response in Ice Infested waters" (Vefsnmo *et al.*, 1996). The ONA research program included information on physical environment, behavior and properties of oil, oil spill response (biological, burning, dispersing, emulsion breaking and mechanical oil recovery). Later work evaluating the status and research needs for future oil in ice research is covered by Dickins *(*2004).

Work to date has led to a good general understanding of the key processes controlling the behavior of fresh and emulsified crude oil in a variety of ice conditions including landfast and broken pack ice. However there is still much to be learned, for example about the detailed processes of oil encapsulation and migration under different climatic conditions, and the behavior of different oil types in a range of possible ice regimes.

1.3 In-situ burning as an Arctic spill countermeasure

The consensus of research on spill response in broken ice conditions is that in situ burning is often a highly effective response technique in both solid and broken ice conditions with removal rates exceeding 85 percent in many situations. Experience includes burning oil on melting solid ice and in pack ice and slush during relatively large field experiments (e.g., Norcor 1975, Dickins and Buist 1981, Shell et al. 1983, SL Ross and DF Dickins 1987, Singsaas et al. 1994). A considerable amount of research has also demonstrated the potential for in situ burning in broken ice. This research included

several smaller-scale field and tank tests (SL Ross et al. 2003, Shell et al. 1983, Brown and Goodman 1986, Buist and Dickins 1987, Smith and Diaz 1987, Bech et al. 1993, Guénette and Wighus 1996) and one large field test (Singsaas et al. 1994).

2. OVERALL PROGRAM SCOPE AND OBJECTIVES

This study incorporated trials of surface and airborne radar and a surface-based acoustics system in a large-scale test under a realistic field setting of natural sea ice. The availability of a relatively large (thousands of liters) crude oil spill under sea ice also provided an opportunity for a new set of measurements and observations on all aspects of oil-ice interaction, including at the end of the project, an assessment of in situ burning and procedures for residue recovery.

2.1 Objectives - Oil and ice detection

The 2004 CRREL tank tests showed that GPR systems could detect and map oil pools as thin as one inch (2 to 3 cm) under controlled conditions under model sea ice up to 16 inches (40 cm) thick (Dickins et al., 2005; Bradford et al. 2005). The Svalbard field experiment created a larger-scale spill under thicker natural sea ice to further evaluate potential remote sensing systems as practical operational tools by expanding the operating boundaries (spill size, ice thickness, airborne measurements). Primary objectives of the remote sensing study components on Svalbard were to:

- Test a second-generation radar system incorporating improvements in reliability and software with crude oil spilled under thicker sea ice (up to 1 m) and over a large enough area to allow airborne (helicopter-mounted) measurements at low altitude in addition to surface 2-D and 3-D surveys.

- Test currently available acoustic technology, building on earlier success in Canadian trials from the 1980's and utilizing the latest processing hardware and software with a new approach to coupling the transducers to the ice surface without the need for direct contact (a major drawback of earlier systems).

In addition, the spill provided an opportunity to further investigate the potential levels of hydrocarbon gases within the ice above trapped oil. The goal was to increase the level of understanding as to whether the flux levels of components such as ethane would be sufficient to support effective surface or airborne detection with more portable and sensitive new-generation gas sensors in the future (such as those developed by Shell Global Solutions and tested in prototype form in 2004).

2.2 Objectives- Oil Fate and Behavior in Ice and Clean-up Effectiveness

In addition to the goal of evaluating and developing operational oil-in-ice detection systems, the 2006 spill added to the understanding of oil behavior in ice and the implementation of effective clean-up strategies. Scientific and engineering objectives in these areas included:

- Documenting the vertical migration rate of oil as a function of air and ice temperatures and ice crystal structure, salinity and brine volume.
- Mapping and documenting oil distribution and spreading under the ice (thickness, area coverage).
- Documenting the rate and extent of oil encapsulation following the spill (any new ice growth beneath the oil).
- Documenting migration of water-soluble components through the ice, and evaporation and possible emulsification on surface melt pools.
- Evaluating the effectiveness of in-situ burning when the oil surfaces.

3. EXPERIMENTAL APPROACH

3.1 SINTEF field station in Svea, Svalbard

SINTEF's field station in Svea, "Polartun", was used as a base for the fieldwork. The field station is well equipped with scientific equipment, laboratories and logistics needed for this type of fieldwork and has comfortable accommodation facilities for a field team up to 30 persons. Svea is the main coalmining site on Svalbard. Through the local mining company, the team had access to additional logistics such as heavy machinery, garages, workshops, welding equipment etc. In addition, the company plane was used to move personnel and critical freight items from Longyearbyen to Svea.

Figure 3.1 shows a satellite image of Spitsbergen with Svalbard and the main community of Longyearbyen in marked relation to the test site. This image was acquired on the day of the spill, March 27 2006. Further images for the winter of 2006 are provided as Appendix D.

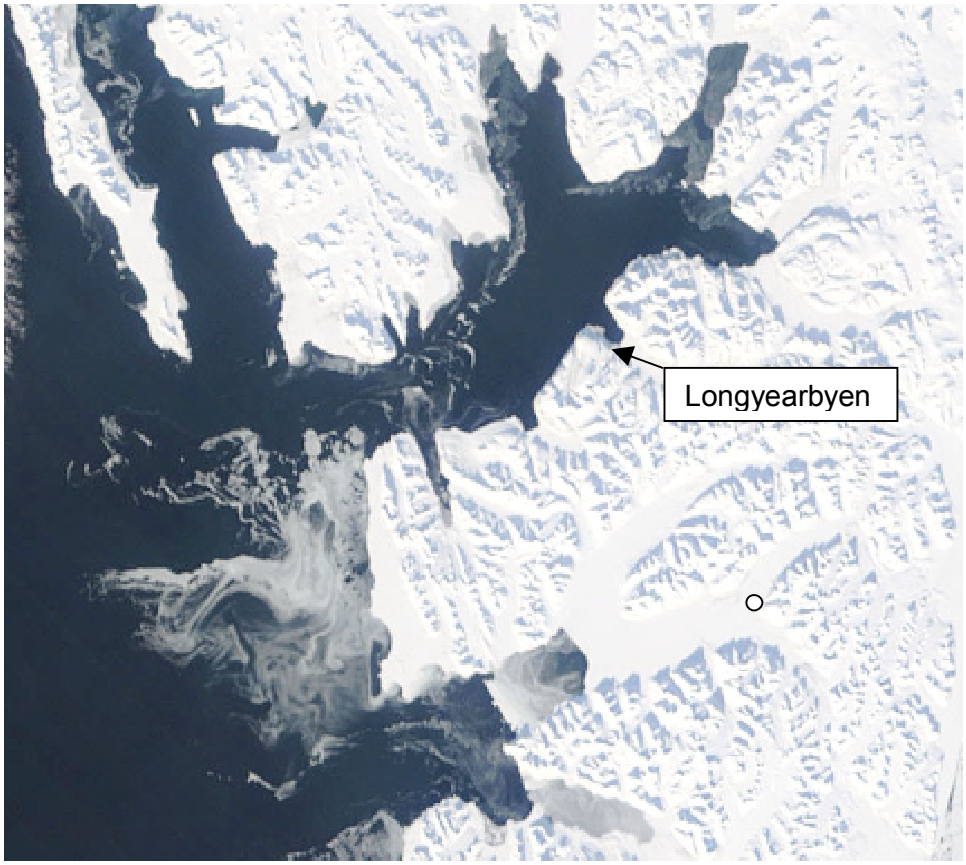

Figure 3.1: The location of the field station and the experimental site ○ in Sveabukta outside Svea, viewed in a NASA MODIS image acquired March 27, 2006. Details for the experimental site are given in Figure 3.8.

Figure 3.2 shows a small-scale map of the fjord area around Svea in relation to the test site.

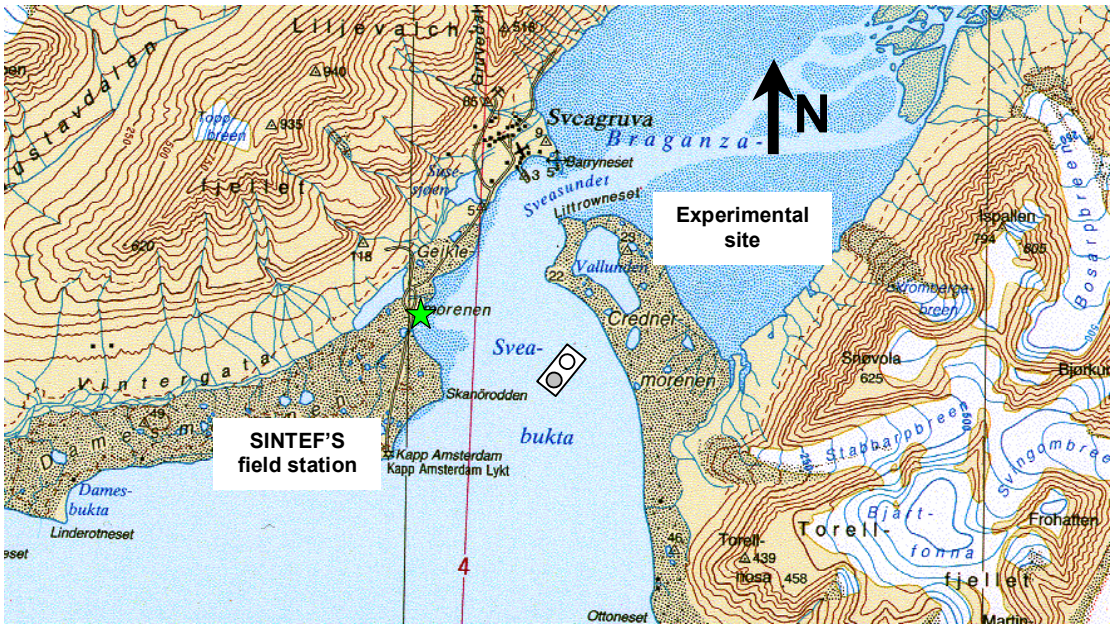

Figure 3.2: The location of the field station and the experimental site in Sveabukta outside Svea. Details for the experimental site layout (approx location marked) are given in Figure 3.8.

3.2 Project team and responsibilities

The project team included following organizations and individuals, with primary responsibilities identified.

David Dickins, DF Dickins Associates Ltd.	Co-coordinator for remote-sensing project components and final report.
Per Johan Brandvik, SINTEF/UNIS	Co-coordinator for oil fate and behavior research and countermeasures evaluation

<u>Oil Fate and Behavior Technical Team:</u>

Kristin Rist Sørheim, Scientist, SINTEF	Oil sampling and analysis
Bror Johansen, Senior field technician, SINTEF	Logistics, dive leader
Frode Leirvik, Senior field engineer, SINTEF	Logistics/sampling, diving
Liv-Guri Faksness, PhD student, UNIS/UiB	Ice/oil sampling and analysis
Roger Daniloff, MSc student, UNIS/NTNU	In-situ burning of oil in melt pools

UNIS – *The University Center in Svalbard*

Remote Sensing Technical Team:

Boise State University, CGISS
John Bradford, Faculty — GPR and acoustic evaluations
Lee Liberty, Faculty
Troy Brosten, PhD Student

CGISS - *Center for Geophysical Investigation of the Shallow Subsurface*

In addition to the field team, Exploration Technologies Inc., Houston, under the direction of Victor Jones provided additional laboratory analysis and interpretation of ice, air and water samples collected during the initial (March) field program, related to gauging the future potential of ethane sensing technologies such as Shell's LightTouch system employed in the earlier 2004 tank tests (Dickins et al. 2005). Refer to summary of these findings in Appendix E.

Six sponsors sent representatives to Svalbard to observe the experimental spill and immediate post-spill sampling and remote sensing tests.

Organization	On-site Representative
MMS	Sharon Buffington
ADEC	Dianne Munson
STATOIL ASA	Gunhild Neverdal
Shell Technology Norway	Gina Ytterborg
Sakhalin Energy Investment Company	James Robinson
Alaska Clean Seas	Lee Majors

3.3 Permits and Approvals

SINTEF was responsible for the permitting and had meetings with the Governor of Svalbard's environmental section in November 2005 explaining the purpose for the project, experimental methods and environmental safeguards with regard to oil spreading, smoke plumes and final clean-up. Valuable feedback from the Governors office was incorporated into the final experimental design used to apply for a permit to spill oil at the test site on January 30, 2006. An invitation was extended in the application for the Government to test the Helitorch ignition system (retained by on Svalbard as part of the oil spill response inventory) but this was not taken up.

A permit to carry out the experiment was granted on February 16, 2006 with the following statements.

> "It is the evaluation of the Governor of Svalbard that the oil will be contained and that the possibility for oil spreading in the marine environment is low. As long as the experiment is carried out as planned, air emission will be the only significant release of harmful substances to the environment.

> It is the Governor of Svalbard's opinion that the outcome of these experiments is important for developing efficient methods to map and combat oil spills in ice infested areas on Svalbard and in the Arctic in general. The conditions in the van Mijen fjord are good for performing such experiments in a safe manner.
>
> Based on these evaluations is this permit given, by the Governor of Svalbard, to release and burn 3500 litres of oil in van Mijen fjorden as described in your application. The authority to give this permission is based on the Svalbard Environmental Act §57, 1b."

Full copies of the application and permit approval letters are contained in Appendix C.

A short field report, written in Norwegian, was delivered by SINTEF to the Governor of Svalbard after the fieldwork was finished, as described in the release permit.

Note: the English text of the permit application and approval letters is based on an informal translation from Norwegian and they should not be viewed as legal documents.

3.4 Remote Sensing Experimental Approach

3.4.1 Radar Test Sequence and GPR System Description

The first task was to test the GPR response, at 500 MHz and 1000 MHz, with the prevailing ice conditions prior to oil emplacement and evaluate the two skirted test cells for suitability. The purpose of these initial tests was to determine which antenna frequency to use for the oil detection test and to select the test cell, which had the best ice/water interface geometry for emplacement of the oil. The reason for the latter evaluation was primarily trying to avoid the situation where thin ice dominated the skirt perimeter thereby leading to an accumulation of oil at the boundaries of the test area at the expense of the center.

The GPR system was a Sensors and Software Pulse Ekko Pro system operating with 500 MHz and 1000 MHz antennas (Figure 3.3). The trace spacing for all ground- based profiles was 5 cm, with a recording time of 50 ns and time sample interval of 0.2 ns and 0.1 ns for the 500 and 1000 MHz systems respectively. System triggering was accomplished using a low friction odometer wheel (Pictures in Appendix B). This triggering system was used previously for a variety of surveys on ice and snow. Experience showed that that there is negligible wheel slippage, resulting in consistent spatial triggering. The radar itself was a new system, not previously tested in the Arctic environment, but the electronics were similar to the system tested in Prudhoe Bay in 2005 and reported previously (Dickins and Bradford, 2005). The system functioned flawlessly and no hardware difficulties were encountered during the field deployment.

Test data were acquired along four profiles with one set of two orthogonal profiles intersecting at the center of each containment cell. From these initial tests without oil, it was concluded that there was no clear distinction in the geometry of the ice/water interface in the two cells but that slightly better data quality was observed in the southern most cell. Additionally, the 1000 MHz antenna did not provide adequate penetration of

the ice to image the ice/water interface consistently, but the 500 MHz system imaged this boundary effectively. Based on these results, the southernmost containment skirt was selected for the oil injection test, and the 500 MHz system was used for the time lapse imaging experiments (discussion following).

To measure the radar velocity for computing the time/depth transform, an *expanding spread gather* was acquired. In this geometry, the source and receiver are moved to successively greater distances apart about a common center point. After picking travel times to the base of the ice reflection, the velocity is found by fitting a line to a plot of t^2 vs. x^2 where x is the source receiver offset and t is the travel time. The velocity is the then the square root of the inverse slope (Figure 3.4). This analysis yielded a bulk velocity for the ice of 0.134 m/ns, which corresponds to a relative dielectric permittivity of 5. This value is typical of that found for sea ice in other locations.

After the initial tests, two separate surface experiments were performed over the oiled ice: 1) 3D imaging over a 20 x 20 m grid centered on the containment area before and after the oil emplacement to identify and map changes in the GPR response, 2) A long 2D profile after oil emplacement to determined the ability to differentiate the oiled area from the background response.

Figure 3.3: Ground based GPR data acquisition along established gridlines with the 500 MHz system.

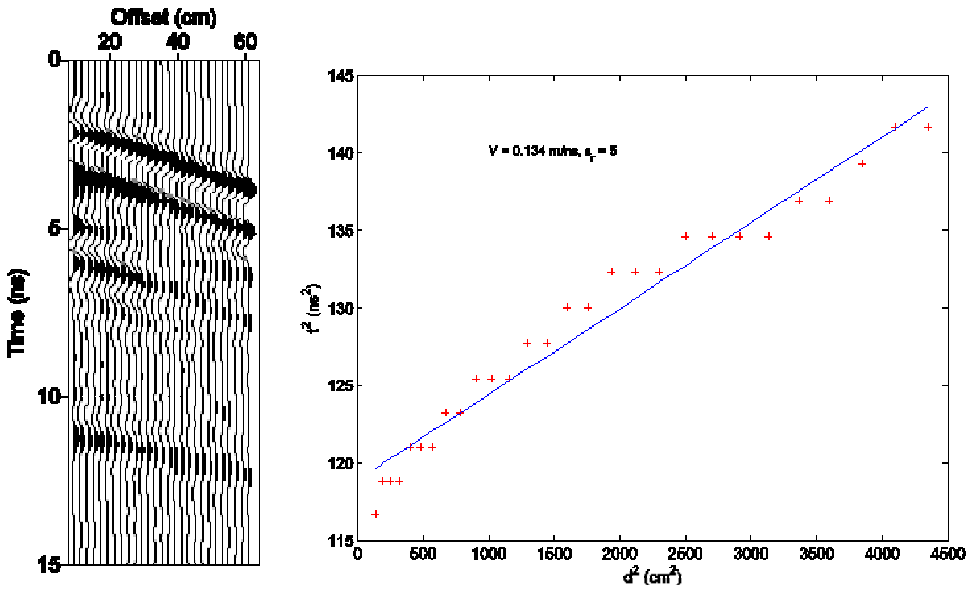

Figure 3.4: Expanding spread profile and plot of t^2 vs. d^2 where d is the offset. The travel times are picked from the first zero crossing of the base of ice reflection that arrives just below 10 ns. The measured velocity of 0.134 m/ns is within the range typically reported for sea ice

Airborne tests from a helicopter-mounted system were conducted at a variety of airspeeds and elevations. For the airborne radar tests, the radar antennas were mounted on a small helicopter between the skids with the base of the antennas at approximately the base of the skids (Figure 4.7). This positioning was critical to minimize scatter from the skids or other metal components of the helicopter. The Pulse Ekko Pro 500 and 1000 MHz antennas are shielded, this served to minimize the amount of energy radiating above the antennas which would then be reflected back down and interfere with the subsurface reflections. Data were acquired across the skirted areas with the parameters noted in Table 3.1. For position control, snow machines were parked along the centerline of the profile at 10 m on either side of the oiled cell and on one side of the control cell. The snow machines produced a clearly identifiable scattering pattern.

Table 3.1: Parameters for airborne tests over oiled areas

Antenna Frequency (MHz)	Height above surface (Meters)	Ground Speed (Knots)
500	3	7
500	5	7
500	10	7
500	5	15
500	10	15
1000	3	7
1000	5	7
1000	10	7
1000	15	7

Results from each of these tests are discussed in Chapter 4.1 Pictures 22 to 26 in Appendix B show the radar measurement field activities.

3.4.2 Acoustic Detection Methods

3.4.2.1 Background and Review of Past Acoustics Research

Past studies suggest acoustic methods show promise in imaging crude oil beneath sea ice (e.g., Jones and Kwan, 1982; Jones et al., 1986). Many of the previous studies focused on identifying and distinguishing compressional wave (p-wave) energy and shear wave (s-wave) energy at all relevant contacts. This approach was taken due to the small velocity-density contrasts between crude oil and sea water, the complexity of sea ice growth (potential for inter-ice reflections), and the fact that reflected shear wave energy from an oil/water contact should be negligible (Jones et al; 1986). Therefore, ratios of reflected p-wave energy to s-wave energy should increase when incidence angles increase. The rationale for this approach was that the low precision digital instruments (early 1980's technology) were not sufficiently sensitive to identify this small contrast in p-wave reflection energy. This approach required source and receiver transducers to be separated by upwards of 1.0 m, freezing the transducers to the ice surface, and confidently separating p-wave and s-wave energy. Slow acquisition and signal processing issues prevented this older technology from advancement.

3.4.2.2 Experimental Approach

This experiment revisits the use of acoustic methods to identify crude oil beneath sea ice. Estimates of physical properties of sea ice, crude oil, and seawater are examined to conclude that the reflection coefficient for an oil/water contact is actually greater than previously reported. The response of a three-layer system is then modeled using physical property estimates of sea ice, crude oil, and sea water under the assumption that only p-wave energy is generated using a vertically oriented transducer source and that mode conversions do not appear at vertical incidence. Modeled results were followed with the Svea field test (discussed in Chapter 4) using a modern marine sonar unit with a narrow directed beam to generate signals at both 50 kHz and 200 kHz. In that test, reflections

from ice/oil, ice/water, oil/water and water bottom interfaces were identified without directly coupling the transducer to the ice surface. This was achieved by applying a thin film of seawater directly to the ice surface, thereby acoustically bonding the transducer to the ice with the advantage of moving the transducer in real time along a smooth ice surface. The presence of upwards of 50 cm of snow on the ice surface prevented the team from making acoustic measurements without first clearing the snow layer, but sufficient measurements were obtained to show that 50 kHz and 200 kHz signals penetrate and return through the ice layer. Reflections that follow the inferred basal ice reflection are associated with an oil/water contact when tests were performed within the containment skirt (over the oil). Although acoustic methods can distinguish the presence of crude oil under sea ice under ideal conditions, in a field environment, varying surface and ice conditions strongly influence reflected signals from below the ice, making unambiguous interpretation difficult. Pictures 27 and 28 (Appendix B) show field activities during the acoustics data collection program.

3.4.2.3 Physical Properties

The seismic reflection coefficient (R) defines the relative amplitude of energy reflected back toward the source to the energy that transmits through a body. Under plane wave conditions, this equation requires both seismic velocity and density values of the contrasting media. The reflections coefficient is defined as:

$$R = (p_2V_2 - p_1V_1) / (p_2V_2 + p_1V_1)$$

Where p is the density for the top (1) and bottom (2) layers, and V is the velocity of layers 1 and 2. A negative reflection coefficient implies a decrease in the velocity-density contrast across an interface.

Sea Ice: Acoustic properties for sea ice can widely vary as parameters such as ice age, origin, and depth vary. Xie and Farmer (1994) observe acoustic velocities that range from 2,500-3,500 m/s for first year sea ice. Shear wave velocities are observed at approximately 50% of P-wave values or 1,500-2,200 m/s. In our study, we looked at the earliest arrivals that represent the initial p-wave reflection from the base of the ice (and potentially inter-ice reflections) and subsequent arrivals from the upper few cm below the base of the ice that would represent an oil/water interface. Vertically oriented transducers transmit primarily compressional wave energy and shear wave signals should be negligible. If pure shear wave energy is present, arrival times would be at roughly two times the travel time of p-wave signals and not interfere with an oil/water reflection immediately below the basal ice p-wave reflector. Additionally, mode converted arrivals (p-s, s-p) should not form when a transducer acts as both the source and receiver at vertical incidence angles. For this study, we used a p-wave velocity of 3,000 m/s for both modeling and discussion of field results.

Sea ice densities can also vary greatly with a range of ice configurations. Soft ice, layered ice, and other ice configurations can strongly influence ice densities. Here, we used estimates by Jones et al. (1986) that suggest first year ice has a density of 0.9 g/cc.

Since acoustic velocities for sea ice are significantly greater than either oil or water and densities are similar to oil and seawater, reflection coefficients at the interface between

solid ice overlying a liquid phase should always produce a strong negative reflection coefficient. The one exception to a strong negative acoustic reflection at an ice/liquid boundary is where a soft ice base may be present. Under these conditions, a more diffuse set of reflections may appear.

Crude Oil: Crude oil acoustic velocity varies as a function of oil density, pressure, and temperature. Oil densities are often measured using American Petroleum Institute values where:

$$\text{API gravity} = (141.5/\ _0) - 131.5$$

Batzle and Wang (1992) define ultrasonic velocity for crude oil as:

$$V_{oil} = 15{,}450 * (77.1 + API)^{-1/2} - 3.7 * T + 4.64 * P + 0.0115 * (0.36 * API^{1/2} - 1) * T * P$$

where P is pressure.

Figure 3.5 shows the relationship between crude oil density and acoustic velocity along a series of temperature curves. Note that an API of 10, oil density is equivalent to fresh water. For the purposes of our modeled results and discussion, we use a seismic velocity of 1,453 m/s. This value is derived from a temperature of -2° C (approximate sea water freezing temperature) for a medium crude oil of 37.8 API or = 0.84 g/cm^3 (crude oil density for Statfjord crude oil spilled at Svea) at surface pressures.

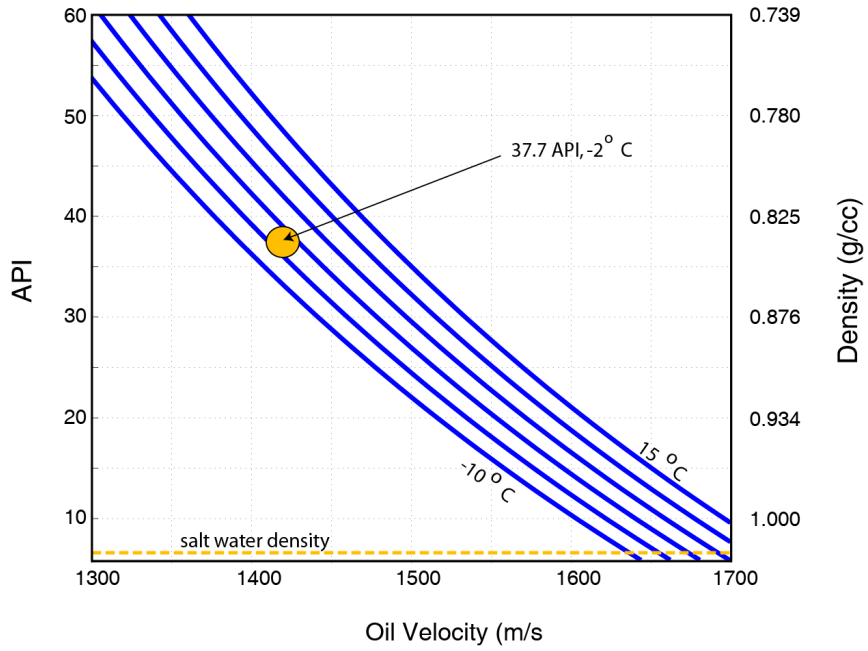

Figure 3.5: Acoustic velocity for crude oil at a range of densities and temperatures. The circle represents the acoustic velocity of 1,453 m/s for API 37.8 crude oil at a temperature of -2° C

Water: Acoustic velocity in seawater varies as a function of water temperature, depth, and salinity. The equation that governs water velocity is:

$$v_w = 1449.2 + 4.6 * T - 0.055 * T^2 + 0.0003 * T^3 + (1.34 - 0.01 * T) * (S-35) + 0.016 * Z$$

where v_w represents water velocity in m/s, T represents temperature in Celsius, S represents salinity in parts per thousand, and Z represents water depth in meters (Sheriff, 2002). Figure 3.6 shows the variation in acoustic velocity as a function of water temperature for both fresh water and seawater at 3.5% salinity. Our modeled results and field tests assume an acoustic velocity of 1,440 m/s using 3.5% salinity water at -2° C at 1.0 m depth. Water density varies as a function of temperature, salinity, and depth. Water density for surface seawater is approximately 1.028 g/cm^3.

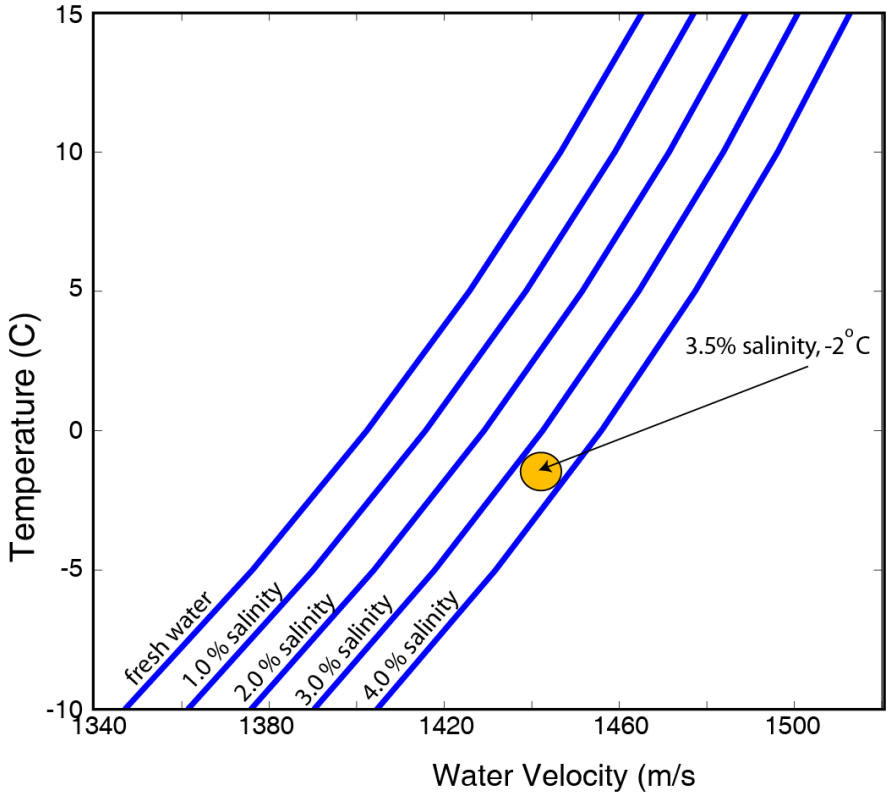

Figure 3.6: Acoustic velocity for water at a range of temperatures and salinity. The circle represents a velocity of 1,440 m/s for water at 3.5% salinity and -2° C.

3.4.2.4 Modeled acoustic results

We discuss two possible scenarios, the presence of crude oil and the absence of crude oil under sea ice. The acoustic properties defined above for ice, oil and water all suggest that a large negative reflection coefficient (R) will appear at either an ice/oil or an ice/water contact. For an ice/water interface, R = -0.292 compared to R= -0.367 for an ice/oil interface. This suggests 29.2% of the energy is reflected back to the surface at an ice/water contact compared to 36.7% of the energy from an ice/oil contact or a 26% change in the amplitude response should appear at an ice/water interface compared to an ice/oil interface. Because of a large density contrast for the Statfjord oil compared to seawater, a positive reflection coefficient appears at the oil/water interface. Here, we observe R=0.0845 at this boundary. This value is more than 4 times the R=0.02 value estimate reported by Jones et al. (1986). Reflection coefficients of this magnitude are routinely measured in seismic reflection and ground penetrating radar studies. The magnitude of the reflection coefficient diminishes as the density of the crude oil increases (lower API). Given a constant temperature and salinity, oil densities would approach fresh water densities (API=10) before no reflection coefficient is present. However, in practice, background noise levels would likely exceed reflected signals for heavy oil.

Next we consider the frequency component of the signal to determine the relative wavelengths of acoustic signals with respect to potential oil thicknesses. Previous studies (e.g., Jones and Kwan, 1982; Jones et al., 1986) determined that frequencies upwards of 200 kHz could penetrate one meter of ice. Within an ice layer at 3,000 m/s, a 200 kHz signal produces a wavelength of 1.5 cm. Wavelengths within both oil and water are approximately 0.72 cm. For a 50 kHz signal, wavelengths within ice and oil/water are approximately 6 cm and 2.9 cm respectively. These values suggest that more than one wavelength will often separate signals between an ice/oil and an oil/water interface given a reasonable spill size. If we can identify the reflector from the base of the ice, we can search for a reflector below this arrival that is of opposite polarity and roughly ¼ amplitude of the ice/oil interface. If thinner amounts of oil are present, diminished amplitudes on the basal ice reflection should result.

Figure 3.7 shows the results of an acoustic finite difference model for a range of oil thicknesses under sea ice using physical properties discussed above. We use a 200 kHz wavelet and appropriate velocity and density values to produce the modeled results. We show the seismic response of the presence of oil thicknesses that range from 0 cm to 10 cm for an API oil density of 37.8. Figure 3.7 shows there are clear wavelet separations from the oil/water interface and the ice/oil interface for all modeled oil thicknesses. Estimates based on a 50 kHz acoustic source suggest oil spills that pool more than 3 cm of oil should be observed with acoustic methods. This is in contrast to the radar methods where the wavelengths are much longer and we rely on thin-bed methods to characterize oil properties (Bradford et al., 2005).

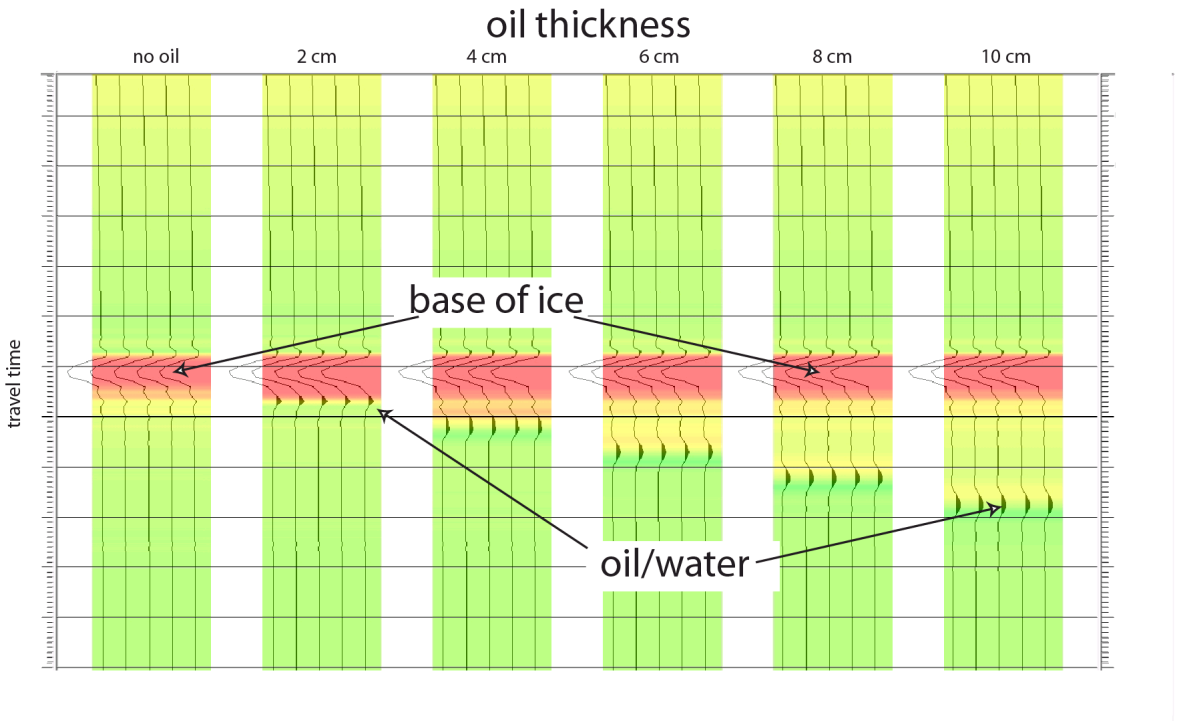

Figure 3.7: Acoustic finite difference model for a three-layer model; sea ice, crude oil, and sea water over a range of oil thicknesses. Note the basal ice contact is represented by a large negative amplitude reflection indicative of the large decrease from solid to fluid acoustic velocities. The oil/sea water contact appears as a positive amplitude reflector due to the increase in density of seawater compared to 37.7 API crude oil. Color represents reflection strength.

3.5 Oil behavior related field activities

These sections contain descriptions of the experimental methods related to documenting the behavior and properties of the released oil, including: migration and weathering processes, results of analytical work performed at UNIS/SINTEF on oil and ice samples, and the in-situ burning operation at the test site.

3.5.1 Preparation for oil release – skirt insertion

In this experiment the oil was held in place under the ice by a circular plastic skirt inserted through the ice. Two spill containment skirts were installed as 11.2m diameter circles (area 100 $m^{2)}$ through 45 cm ice, February 20-22 (see Picture 1 and Picture 2 in Appendix A). Total skirt material length was 40 m to allow sufficient overlap. The skirt depth of 150 cm allowed for ample material hanging beneath the ice. Pockets were sewn into the skirt to contain 2x4" wooden flotation rods on top, and small iron bars to weight the bottom (invisible to the radar signal).

Two test areas (one intended for the spill and one as a control) were installed in line with the prevailing wind direction approximately 30 m apart (Figure 3.8).

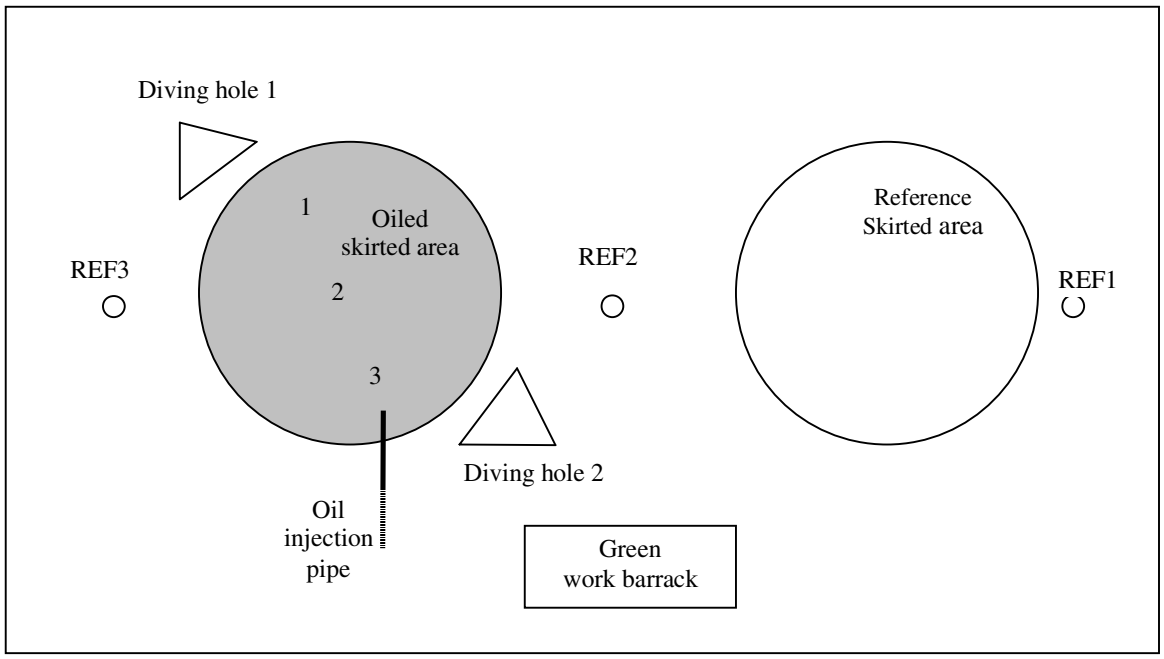

Figure 3.8 The relative position of the two skirted areas and the sampling positions. The shaded area was holding the oil; the other was used as a reference. The numbers between the areas (REF1-3) show the location of the reference ice. The numbers inside the oiled area show the shallow ice cores (upper 20cm) taken two days after the oil was released (March 29). Core numbers 2 and 3 were sent to Houston for independent analysis of trapped hydrocarbon gases– see Appendix E)

3.5.2 Oil release

SINTEF field engineers started to prepare for the oil release in mid March. The full field team arrived in Svea on March 24 and 25 after completing safety training (lectures and firing range practice) at UNIS in Longyearbyen. On-site representatives from the oil companies received their safety training in Svea. Conditions on site improved markedly from the 25th on, and moderate to low winds and clear skies favored the remaining test period. In compliance with the terms of the spill permit (Appendix C), underwater camera surveys were conducted around the skirt at six points to confirm that the skirt was hanging evenly beneath the ice with no kinks or openings for the oil to flow out (*Figures 3.9 and 3.10*).

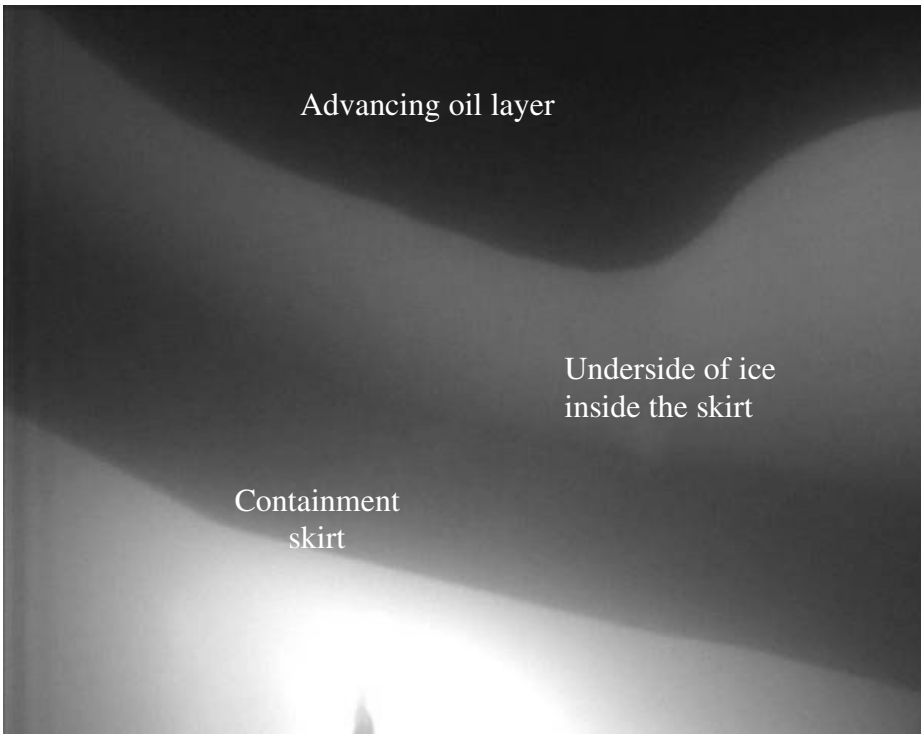

Figure 3.9: Underwater photo showing the inside of the skirt and the advancing layer of oil during the oil release.

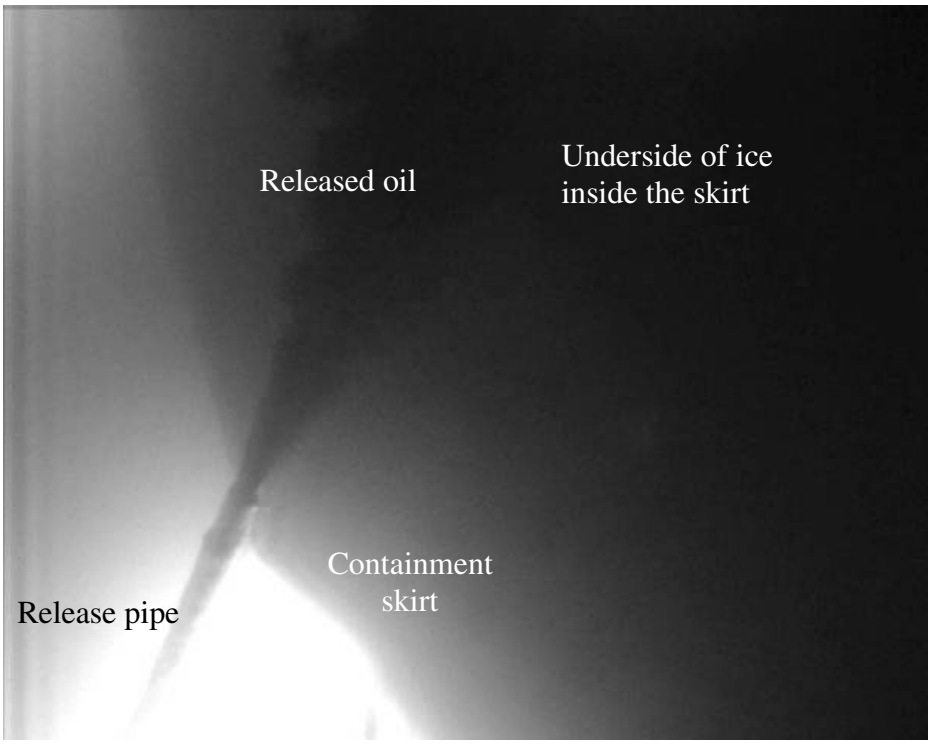

Figure 3.10: Underwater photo of the oil release pipe during the release. The dark shadow above the pipe is the containment skirt.

The spill took place as scheduled on March 27, 2006. Oil was injected under the ice through a neutrally buoyant pipe inserted through an augur hole drilled at an angle just outside the skirt. A total of 3,400 liters (18 drums) of Statfjord crude was pumped from drums over a period of 2 hours and ten minutes (see Picture 3 in Appendix A). The air temperature at the time was -15°C and the oil was at ambient. No difficulties were encountered in the pumping and no oil was spilt on the ice/snow at the site.

The progress of the oil injection was monitored and recorded by an underwater camera focused on the end of the injection pipe approximately 1 meter inside the skirt. The same camera was periodically moved to different inspection holes around the skirt perimeter to monitor the progress of the advancing oil boundary as the test area approached 90%+ coverage (*Figure 3.9*). No oil was observed outside the skirt during and after the oil injection by the underwater camera or no sheen was observed in the inspection holes outside the skirt. However, a band of fine oil droplets (0.2 to 1 mm diameter) was observed approximately 2.5 cm from the bottom of a core taken at Ref 3 location (*Figure 3.8*) 48 hours following the spill (Section 4.3.2).

Basic physical/chemical properties of the fresh Statfjord crude released under the ice are given in the Table 3.2 below.

Table 3.2: Basic physical/chemical properties of the fresh Statfjord crude (1990)

Analysis	Value	Method
Density (g/ml, 15.5ºC)	0.8340	ASTM-method D4052-81.
Pour point (ºC)	-6	ASTM-method D97-66, IP-method 15/67
Wax content (wt.%)	4.1	Insol. in 2-butanon/diklormetan at -10°C
Asphaltenes (wt.%)	0.01	IP-method 143/84.
Viscosity (cP, shear rate $100s^{-1}$, 13ºC)	7.0	Physica MCR 300

The Statfjord crude is a light paraffinic crude with a relatively low pour point. This oil was stored in Svea on drums for some years but no significant amount of residue was observed in the empty drums after the oil was released. No problems with wax precipitation were observed during the oil release.

3.5.3 Sampling ice cores

A series of pre-spill ice cores were taken at various locations outside the test skirts (see REF 1-3 in *Figure 3.8*) and packed for shipment to the UNIS laboratory in Longyearbyen (ice structure and oil analysis), SINTEF laboratory in Trondheim (oil and water-soluble components) and the ETI labs in Houston (trapped h.c. gas analysis at REF3 location only). A typical ice core drilling operation is shown on Picture 4 in Appendix A.

The ice cores analyzed at UNIS/SINTEF were kept frozen during transport and stored at UNIS ice-laboratory in Longyearbyen. The samples were melted/extracted at UNIS and only the DCM extracts were transferred to SINTEF for analysis.

The ice cores sent to ETI Houston were divided into sections and transferred to screw cap sealed plastic (HDPE) containers. The melted samples were stored in Svea for a few days, transported to Longyearbyen and sent to Houston (see Appendix E for summary of analysis results).

Several sets of ice cores and water samples were taken on March 29 two days after the oil release. These samples included three cores through the top 20 cm of the ice inside the test area (see location 1-3 inside oiled skirted area in *Figure 3.8*). These cores were also divided between ETI and SINTEF/UNIS. Additional reference samples (see REF1-3 in *Figure 3.8*) were also taken on April 20 and May 10 (analyzed only in Norway).

The cores used for salinity measurements were drilled by a team of UNIS students (Aardahl, 2006) at the same site in Svea at five different dates (weeks 8, 9, 11, 13 and 16). The cores were cut in pieces of 0.05 m of thickness from top to bottom, and taken back to UNIS, Longyearbyen. The cores were stored in UNIS' cold lab (-20°C) before they were used for making thin sections of selected cores. Horizontal and vertical sections were cut and glued with distilled water to glass plates. The sections were planed by machine until they had a maximum thickness of 0.5 mm. Then they were studied and pictures were taken through plane polarized light (*Figures 4.15 and 4.16*). The salinity was measured on similar 0.05m sections with a calibrated conductivity instrument (distilled water and conductivity standards – *Figure 4.14*).

3.5.4 In-situ measurements of oil film thickness

To verify the oil distribution inside the skirt, divers were used to measure the film thickness under the ice. Diving operations took place on three different occasions between March 27 and 29. All diving operations were performed according to SINTEF and national regulations concerning the safety standards for professional diving operations under ice (underwater communication, independent spare air supply, standby diver etc.).

Divers entered the test area through two triangular diving holes cut in the ice just outside of the spill skirt (see Picture 5 and Picture 7: Appendix A). A novel under-ice thickness sensor was tested and used successfully to measure the oil thickness at different locations reached from two separate dive holes (see Picture 8: in Appendix A).

In total, 25 thickness measurements (with three replicates each) were taken under the ice. The three parallel measurements from each location were transferred from the diver to the diving leader on the ice by radio. Observations and underwater photographs were taken to show the appearance of the oil layer and the progress of new ice growth at the edge of the oiled area within 48 hours of the spill (see Picture 9: in Appendix A).

3.5.5 Oil weathering

Most of the field crew and observers left for the Norwegian mainland and US a few days after the oil was released and the initial sampling and radar work was finished. A small field crew from SINTEF/UNIS returned to Svea after the Easter holidays (MsS student Roger Daniloff and field assistant), observed the site and collected ice cores and oil samples for weathering studies until May 30. This site monitoring was also needed to avoid interactions with wildlife and unwanted oil spreading, as described in the release permit. Liv-Guri Faksness and Per Johan Brandvik visited the site and collected samples at April 20, April 29, May 10, and finally on May 30 2006 for the in-situ burning operation.

3.5.6 Laboratory work – oil analysis

Quantitative analysis used gas chromatographic-flame ionization detection (GC-FID) and coupled gas chromatographic - mass spectrometry (GC-MS) of the oil or ice core extracts to quantify oil components. This was done to study compositional changes in the oil as a function of weathering and to quantify water-soluble components in the ice core extracts.

The components analyzed (see Table 3.3) were selected for their environmental significance (aquatic toxicity), physical properties (medium water solubility and vapor pressure) and the need for data on concentrations related to oil entrapped in ice (see also Faksness et al. 2004). Earlier studies have shown that these components leak out from oil captured in ice and establish significant concentration gradients through a one-meter thick ice layer (Faksness and Brandvik 2005 and Faksness et al. 2006). This type of data forms an important input into modeling the environmental impact of oil spills in ice (e.g SINTEF OSCAR model).

Concentration of the individual organic compounds (semi volatile organic compounds, SVOC) listed in Table 3.3 were determined using GC-MS. The samples were also analyzed to determine the total extractable organic compounds (TEOC) concentration using GC-FID.

<u>GC-MS Analysis (Modified EPA Method 8270)</u>
Gas chromatography-mass spectrometry (GC-MS) was conducted using an Agilent 6890 Plus GC interfaced to an Agilent 5973 MSD. The GC was equipped with a 60m x 0.25mm ID, 0.25 µm film thickness, HP-5MS capillary column. The mass spectrometer was operated in the selective ion-monitoring (SIM) mode for optimum sensitivity and specificity. The oven program employed was 40°C (1 min), then 6°C/min to 300°C (hold 20 min). Helium was used as the carrier gas.

Prior to sample analysis, the GC/MS was tuned with perfluorotributylamine (PFTBA). An eight-point initial calibration consisting of selected target compounds was established to demonstrate the linear range of the analysis and to determine the mean relative response factor (RRF) for the individual compounds.

The response factors were generated for all targets and surrogates versus acenaphthene-d_{10}. Analyte concentrations in the standard solution ranged from 0.01 µg/mL to 10 µg/mL.

Table 3.3: Target PAH and PAH groups analyzed by GC/MS-SIM.

Target PAH/PAH groups	Abbreviation	Target PAH/PAH groups	Abbreviation
Decalin	DE	C2-dibenzothiophenes	D2
C1-decalins	DE1	C3-dibenzothiophenes	D3
C2-decalins	DE2	C4-dibenzothiophenes	D4
C3-decalins	DE3	Fluoranthene	FL
C4-decalins	DE4	Pyrene	PY
Benzo(b)thiophene	BT	C1-fluoranthenes/pyrenes	FL1
Naphthalene	N	C2-fluoranthenes/pyrenes	FL2
C1-naphthalenes	N1	C3-fluoranthenes/pyrenes	FL3
C2-naphthalenes	N2	Benz(a)anthracene	BA
C3-naphthalenes	N3	Chrysene	C
C4-naphthalenes	N4	C1-chrysenes	C1
Biphenyl	B	C2-chrysenes	C2
Acenaphthylene	ANY	C3-chrysenes	C3
Acenaphthene	ANA	C4-chrysenes	C4
Dibenzofuran	DBF	Benzo(b)fluoranthene	BBF
Fluorene	F	Benzo(k)fluoranthene	BKF
C1-fluorenes	F1	Benzo(e)pyrene	BEP
C2-fluorenes	F2	Benzo(a)pyrene	BAP
C3-fluorenes	F3	Perylene	PE
Phenanthrene	P	Indeno(1,2,3-c,d)pyrene	IN
Anthracene	A	Dibenz(a,h)anthracene	DBA
C1-phenanthrenes/anthracenes	P1	Benzo(g,h,i)perylene	BPE
C2-phenanthrenes/anthracenes	P2	Phenol	PH
C3-phenanthrenes/anthracenes	P3	C1-Phenols	PH1
C4-phenanthrenes/anthracenes	P4	C2-Phenols	PH2
Dibenzothiophene	D	C3-Phenols	PH3
C1-dibenzothiophenes	D1	C4-Phenols	PH4

GC-FID Analysis (Modified EPA Method 8100)

Gas chromatography-flame ionization detection (GC-FID) was conducted using a Hewlett Packard Agilent 6890 Plus GC, both equipped with a 30m x 0.25 mm ID, 0.25 µm film thickness, HP-5 capillary column. The oven program employed was 40°C (5 min), then 6°C/min to 310°C (hold 10 min). Hydrogen was used as the carrier gas.

Prior to sample analysis a six-point calibration was performed to demonstrate the linear range of the analysis. The calibration solution was composed of selected aliphatic hydrocarbons within the n-C_{10} to n-C_{40} range, including pristane and phytane. Analyte concentrations in the standard solutions ranged from 1 µg/mL to 100 µg/mL.

In this study, so far, the GC-FID analysis has been used as a screening of the samples, and little use has been made of the quantitative GC-FID data.

3.5.7 In-situ burning

The oil, being confined under the ice by the skirt, was expected to migrate upward through the brine channels in the porous first year ice. The porosity of the ice is strongly dependant on the air temperature and solar radiation. The first oil was visually detected on the ice surface, under the snow, on April 20 (see Picture 12 in Appendix A). The oil then gradually formed a visible melt-pool on the ice surface. Preparations were made for in-situ burning on May 10, but investigations showed that one third of the oil volume (approx. 1000 liters) was still captured in the ice (see Fig. 4.20). Finally, on May 30 all the oil was considered available on the surface and the oil was ignited and burned. This activity was performed to both test and document in-situ burning as a countermeasure technique and for practical reasons to significantly reduce the volume of oil that needed to be recovered.

The weather conditions were favorable for in-situ burning with calm winds (<2 m/s), an air temperature of 4ºC and a seawater temperature directly beneath the oil of 0ºC. The Statfjord crude was ignited using 100 ml slab of gelled n-hexane ignited with a propane torch. The entire slick was ignited after 2.5 minutes and the burn lasted for 11 minutes. The residue was cooled for 2 hours and was easily recovered manually. The site was treated with sorbent after the residue was recovered. The in-situ burning activities are shown as Picture 16 to Picture 21 in Appendix A.

4. Data and discussions

4.1 Radar measurements

Refer also to Pictures 22 to 26 in Appendix B.

4.1.1 3D surveying

Three-dimensional (3D) GPR surveys were conducted before and after oil emplacement. The data were acquired along 42 profiles in an orthogonal grid with 21 profiles in each direction (Figure 4.1). The orthogonal grid was important to test for azimuthal anisotropy in the GPR response related to preferred orientation of ice crystal formation. The total grid size was 20 x 20 m with GPR profiles on 1 m centers, with an inline trace spacing of 5 cm. After setting the four corners of the survey area, the start and end position of each profile was marked by hammering a 30 cm spike into the ice at each end. Repeatability outside the containment cell was compromised by the need to cut dive holes after the background dataset was acquired. While this effect is certainly evident in the data, it did not affect the response significantly within the target area. Data were acquired continuously by reversing the direction of acquisition for every other profile (Figure 4.1 acquisition template).

Data processing included a time zero correction to account for system padding and drift, a high pass filter (sliding median subtraction with window width equal to twice the period at the characteristic antenna frequency), and relative amplitude gaining (data scaled to t^2). Additional processing steps included subtracting the background data from the data acquired after oil emplacement. This step highlights reflection amplitude changes due purely to the presence of oil. The differencing step was done by taking the absolute value of the Hilbert transform of the data. The Hilbert transform is a complex representation of a time series, and its computation allows computation of the total energy contained in a signal, the phase or shape of the signal, and details of the signal spectrum. This operation is a better measure of the total reflected energy and eliminates effects due to phase rotation of the recorded waveform that may be induced by the introduction of a layer that is thinner than the wavelength of the signal.

Figure 4.2 shows cross sections of the data before and after oil emplacement acquired along x = 7 m in the y-direction (Figure 4.1 page following). Before oil emplacement, a topographic high (or relative thin ice area) is evident at low values of y between x=5 and 9 m. This created a preferred oil accumulation zone and the thickest oil films were measured by divers in this area (see Figure 4.21). After oil emplacement, the reflection from the base of the ice within the containment skirt undergoes a 180° phase rotation. This obvious change in the reflectivity occurs because crude oil has a much lower dielectric permittivity (K~2) than either sea ice (K~5) or seawater (K~87) so that displacement of sea water with oil significantly alters the dielectric permittivity structure of the system. The reflection coefficient changes from positive to negative at the base of the ice since oil has a higher velocity (lower permittivity) than ice or water. The reflection from the base of the oil pool is also evident along this profile as a low amplitude reflection with the same polarity as the ice/water interface reflection outside the containment area.

As the oil thins toward larger x and y values, the oil film is no longer clearly resolved, but we recorded a reflectivity anomaly that is a tuning response due to the presence of the oil film. At x=10 m (Figure 4.3) it is clear that there is a significantly different GPR response within the test cell, with much lower reflection amplitude from the ice water interface within the test cell prior to oil emplacement. There appears to be significant scattering at this interface. This is consistent with the ice water interface being significantly rougher within the test cell. A possible interpretation is that water currents within the test cell are altered because of the containment skirt protruding into the water column, which may allow for more irregular crystal growth.

Figure 4.4 shows the amplitude difference from background along the profile at x= 12 m which clearly highlights the oil induced reflectivity anomaly. This tuning response occurs in areas where the oil film is thinner than about ½ a wavelength of the signal (~13 cm) and is a maximum at ¼ wavelength (~7 cm).

A map of the GPR response to the oil emplacement is created by slicing the difference volume horizontally at the ice-water interface (Figure 4.5). The relative distribution of the reflectivity anomaly is consistent with the mapped distribution of oil. Higher reflectivity changes correlate with the tuning response where the oil is on the order of ½ wavelength or less. From the control data and amplitude difference map, it appears that the minimum detection limit is on the order of 1-3 cm, however the sparse distribution of oil thickness measurements prevents a detailed analysis. This result is consistent with our analysis of 500 MHz data from the controlled test at CRREL completed in 2004 (Dickins et al., 2005).

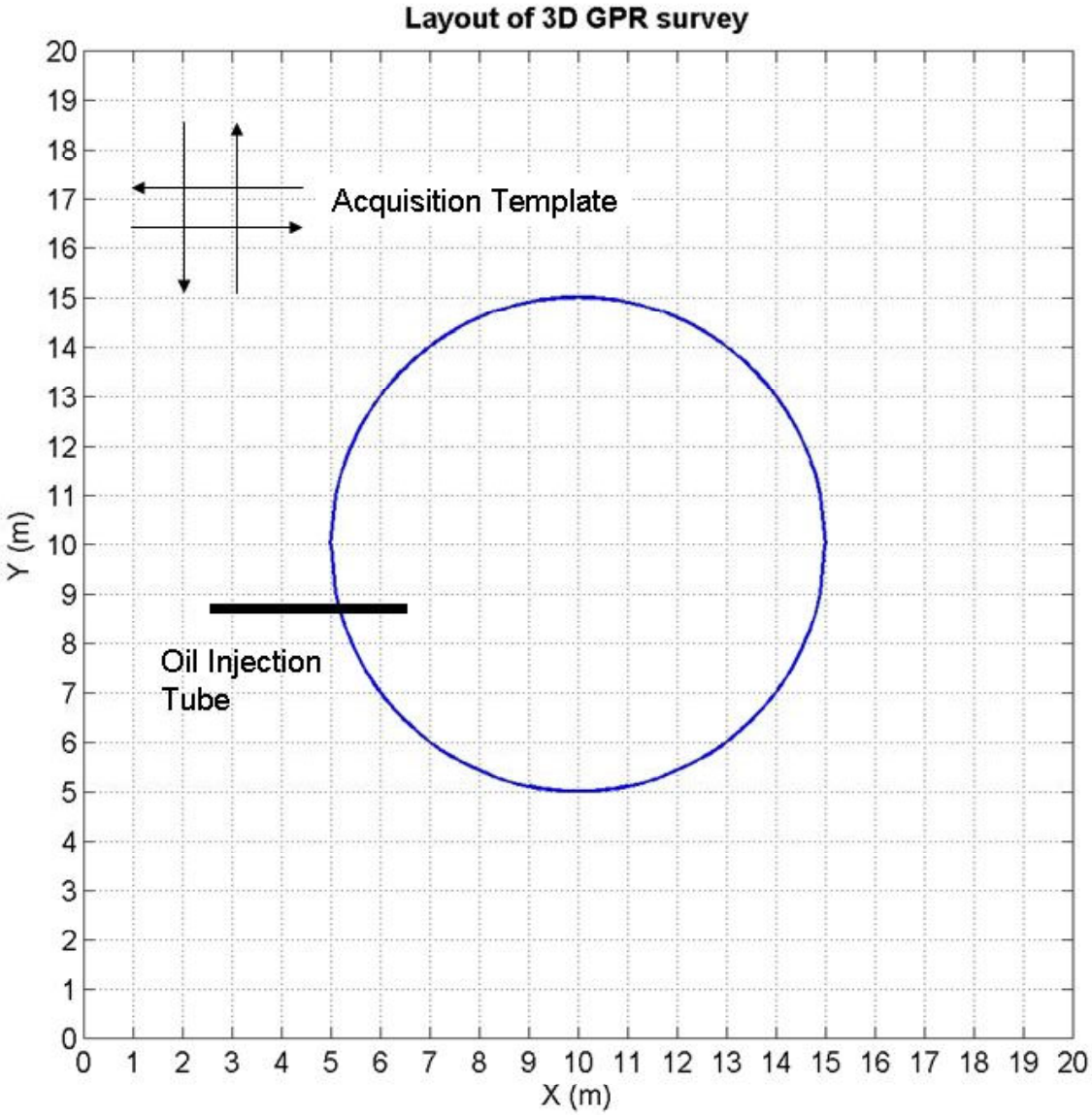

Figure 4.1: Layout of the 3D GPR grid. Data were acquired on 1 m centers on an orthogonal grid. The acquisition direction was reversed for every other profile to allow for continuous acquisition. The data were resorted to the correct relative orientation in post processing.

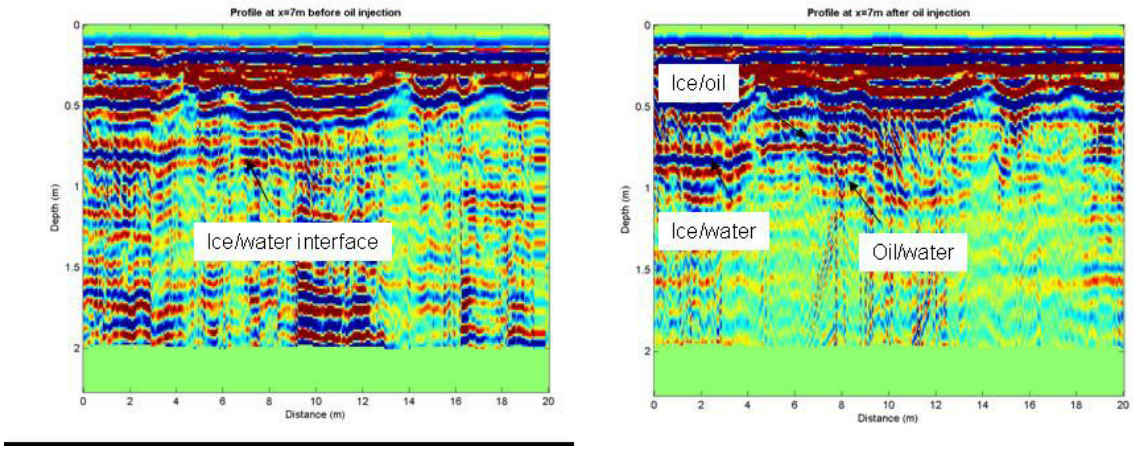

Figure 4.2: Image before and after oil emplacement along x=7m. There is poor data quality on the right hand side of the image with low reflection amplitude from the ice water interface. There is a topographic high (thinner ice) evident at the ice water interface prior to oil emplacement. This creates a space for oil to pool and is the location of the greatest measured oil thickness. After oil emplacement the top and bottom of the oil are resolved.

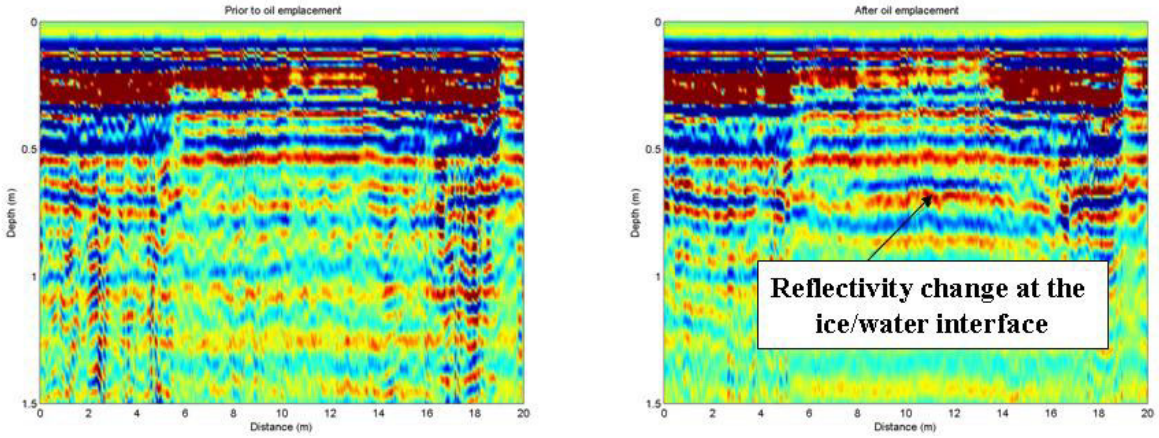

Figure 4.3: GPR reflection images along x = 10 m before and after oil emplacement. The ice/water interface reflection occurs at a depth of about 0.65 m. At this location, the oil thickness is close to ¼ wavelength at 500 MHz and the change in reflectivity is caused by interference between the top of oil and base of oil reflections. Several intra ice reflections are evident, the most prominent occurs at approximately 0.5 m and appears to correlate with the transition to clear slower growing ice with columnar crystal alignment noted in UNIS' thin section analysis.

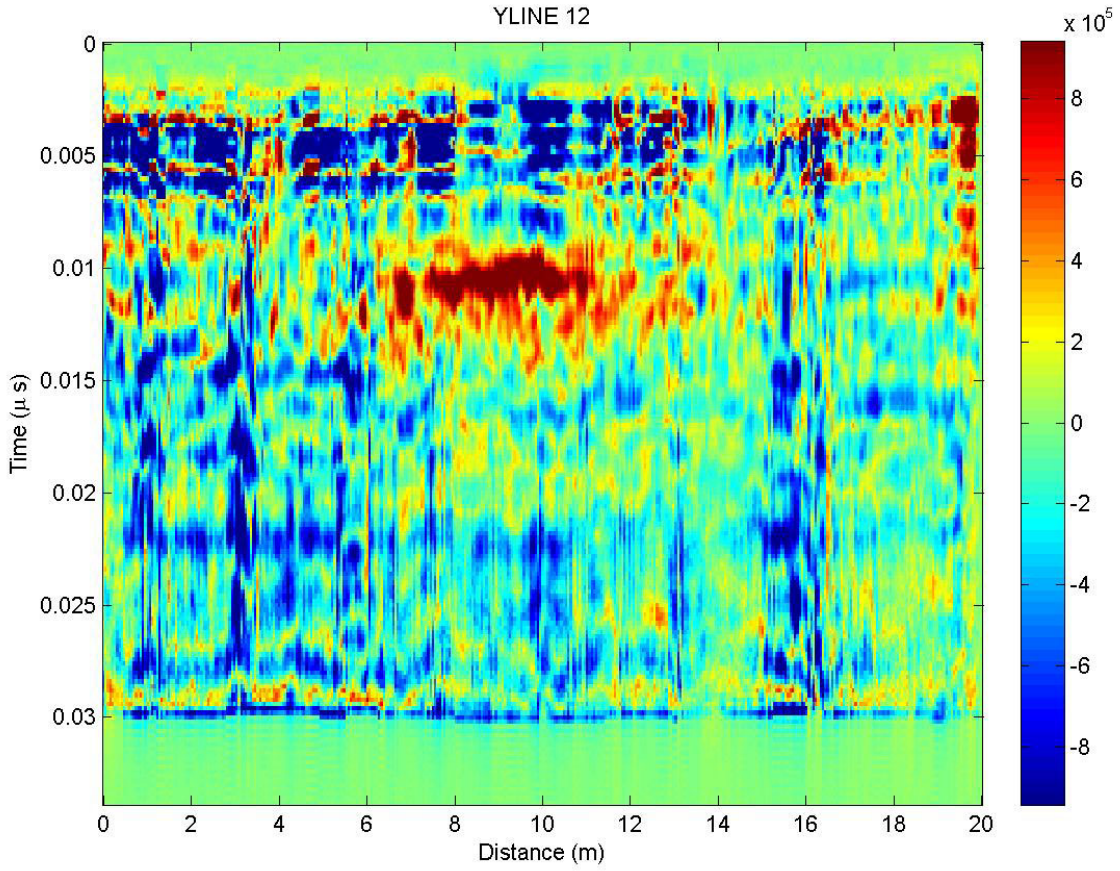

Figure 4.4: Difference image at x=12 m. The oil-induced change is obvious as a large high amplitude anomaly near the center of the profile at 0.01 microseconds.

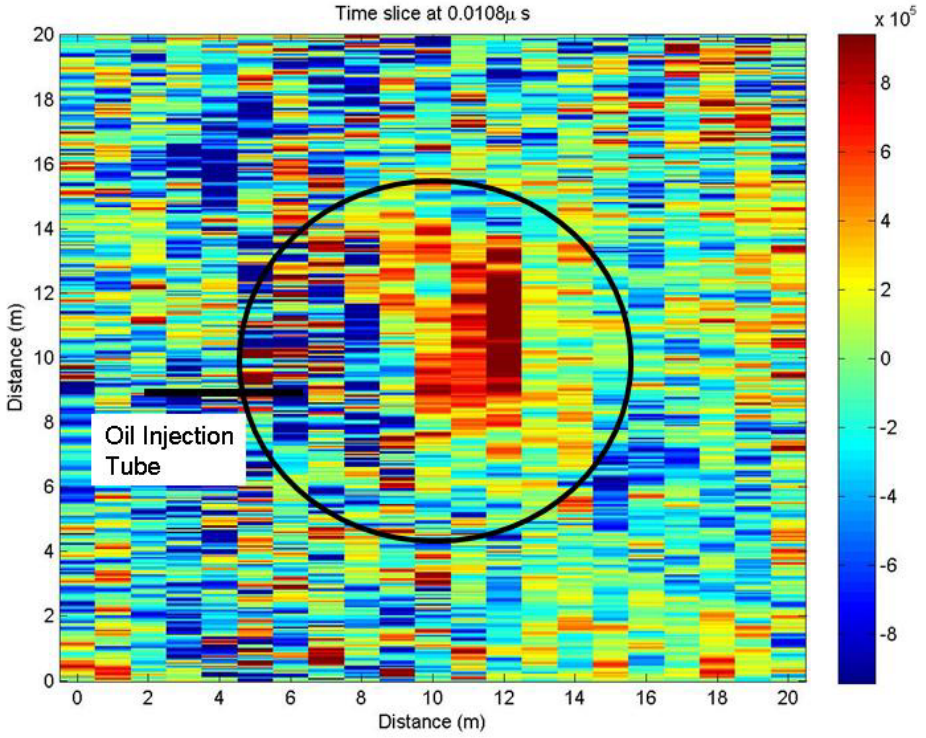

Figure 4.5: Horizontal slice through the differenced volume at t=0.01 microseconds. The largest positive difference occurs along the profile at x=12 m where the oil film is relatively thin and there is a tuning response. On the left side of the cell, where the oil thickness is greatest near the injection point, amplitudes are generally lower after oil injection, but in this area, the top and bottom of the oil layer are resolved. There is substantial phase rotation throughout the volume. Refer to Fig. 4.21 for diver measurements.

4.1.2 Long-scale 2D profiling

To test whether the GPR response to oil within the containment cell could be differentiated from the background response we acquired a 100 m long profile that spanned both contained areas in the y direction. The change in amplitude response, which although obvious in the before and after images in the 3D dataset, is not outside the range of natural variability observed in the long profile. However, the phase of the reflection from the ice water interface within the oiled area differs substantially from the background response. This is evident in the processed reflection data (Figure 4.6). A data attribute transform was found that highlights this variability. The amplitude of the vertical derivative of the reflection data multiplied by the polarity of the derivative is a measure that highlights large gradients in the reflection response and indicates if those gradients are positive or negative. This transform produces an attribute plot that clearly differentiates the oiled zone from the background response along the base of ice reflection. *Note that this plot is relatively noisy above the base of ice reflection. It is important to know the arrival time of the reflection (from the processed reflection image) prior to interpretation.*

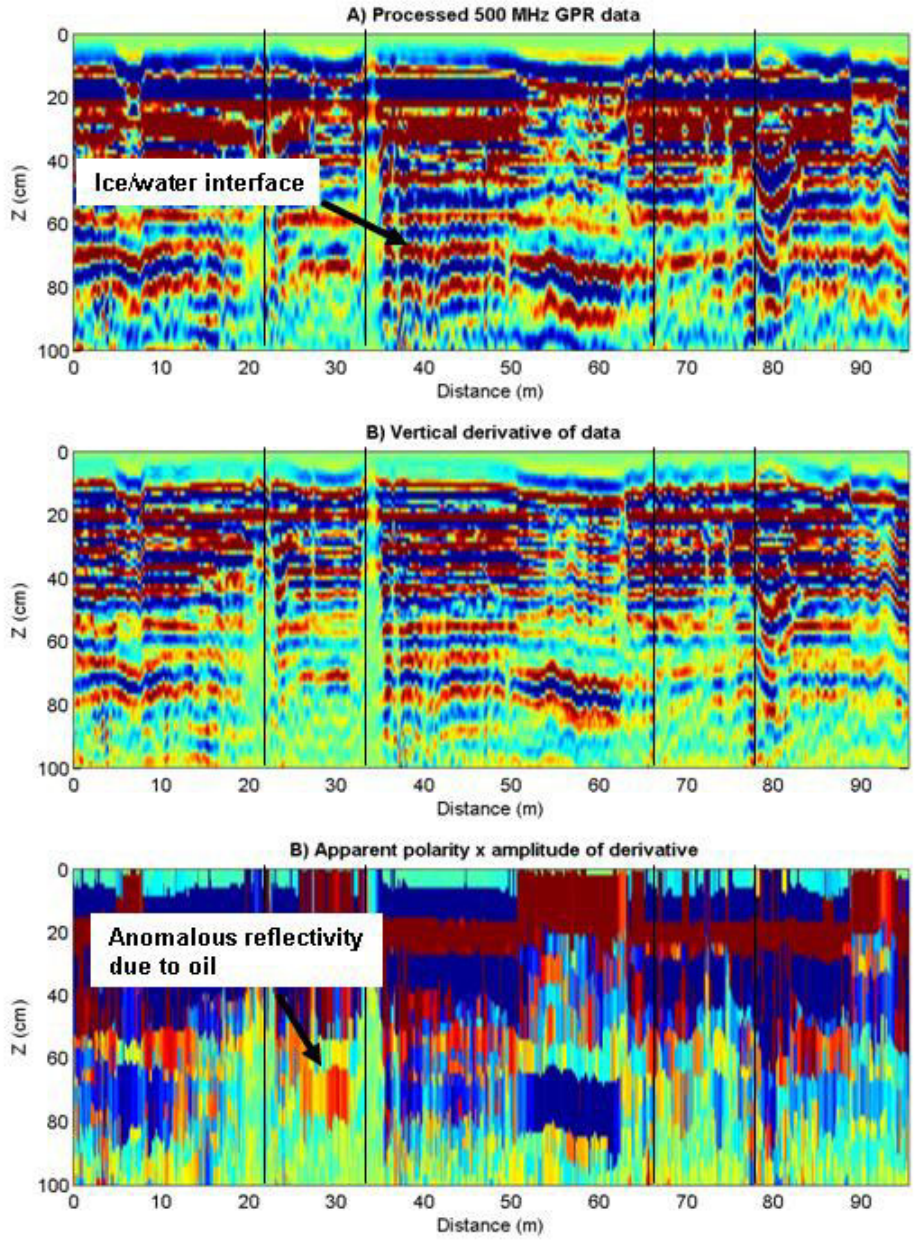

Figure 4.6: Long profile acquired across both containment areas after oil emplacement. The containment skirts are indicated with black vertical lines. The amplitude variation due to presence of oil is similar to the background variability but the phase, or shape of the waveform varies significantly. The apparent polarity multiplied by the amplitude of the derivative highlights this anomaly. Note that these data have been flattened along the snow/ice interface.

4.1.3 Airborne radar tests

For the airborne radar tests, the radar antennas were mounted on a small helicopter (Figure 4.7). Initially, it was concluded that the radar system did not produce adequate energy to reach the base of ice interface. After reprocessing to remove coherent (unwanted) noise caused by close proximity to the helicopter, the results are promising. The additional processing steps included construction of a spatially varying background noise removal filter. This process effectively attenuated helicopter related noise.

Since the helicopter did not fly at a constant altitude, it was necessary to correct the data to a constant datum. The reflections from both the top of snow and snow/ice interface were clearly resolved in both the 500 MHz and 1000 MHz data. Assuming the snow/ice interface was approximately flat, a time shift was applied to the data to flatten this horizon. The resulting sections are comparable at a given frequency for each of the parameter sets noted in Table 3.1. The results of the 500 MHz test at 5m altitude and 7 knots forward speed are shown in Figure 4.8. A coherent event is evident that has the same two-way travel time as that for the base of ice reflection interpreted from the ground based data. Further, the phase rotation is apparent along this horizon within the test cell containing oil. This event is likely the reflection from the base of ice. However, a number of coherent events are evident below this horizon that have similar (low) amplitude. These events are likely due to reverberation within the ice layer (also known as peg leg multiples). However, this response is somewhat ambiguous and further testing is necessary. A higher powered airborne radar system, potentially with beam steering capability to minimize out-of-plane scatter may be necessary to provide consistent unambiguous results (proposed study for MMS sponsorship in 2007).

The 1000 MHz system in airborne mode provided a detailed image of the snow pack and the snow ice interface. A long (~1 km) profile was acquired seaward along the fjord at a height of 10 m and ground speed of 15 knots. A 350 m section of this profile is shown in Figure 4.9 and shows a clear image of the snow pack which varied from ~ 10 – 50 cm along the line. Note that a reflection from a depth of approximately 20 cm within the sea ice is also imaged in this profile. A second profile was acquired over the moraine adjacent to the test cells with comparable parameters (Figure 4.10). This profile shows a clear image of the snow pack thickness that varied from 0 – 200 cm along the profile. Additionally, details of the snows internal stratigraphy are clearly imaged in both profiles. These data demonstrate that there is high potential for high frequency radar to image oil spills on top of sea ice but beneath the snow pack.

Figure 4.7: *The airborne system configured with the 500 MHz antennas, which are visible between the skids. The antennas are connected via coaxial cables to the recording system within the cabin.*

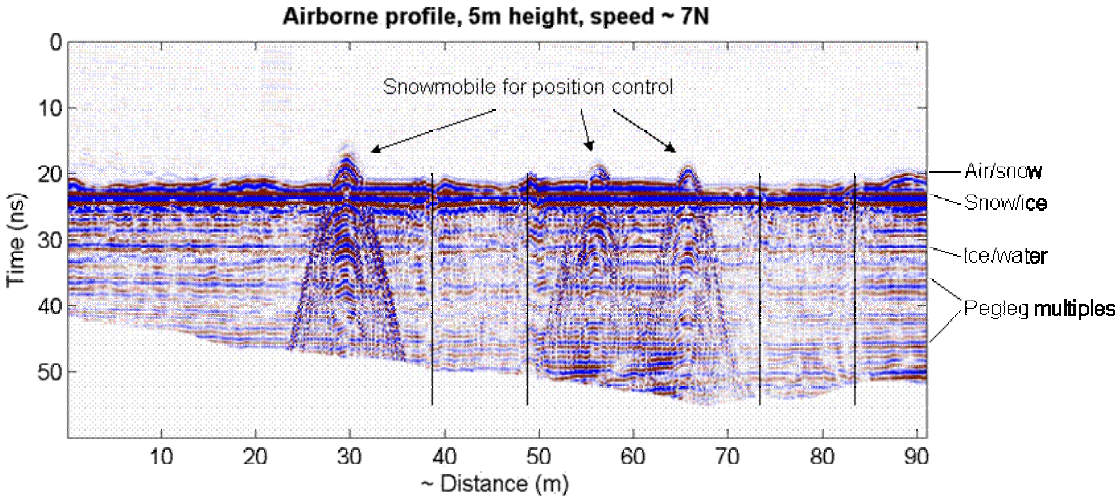

Figure 4.8: *Data acquired over the test cells using the 500 MHz airborne configuration. The phase rotation from the base of ice reflection is evident in the oiled cell on the left. The interpretation is somewhat ambiguous due to the presence of reverberation with comparable amplitude to that of the event interpreted as the base of ice. This may be multiples from within the ice column. The data were flattened to the snow/ice reflection.*

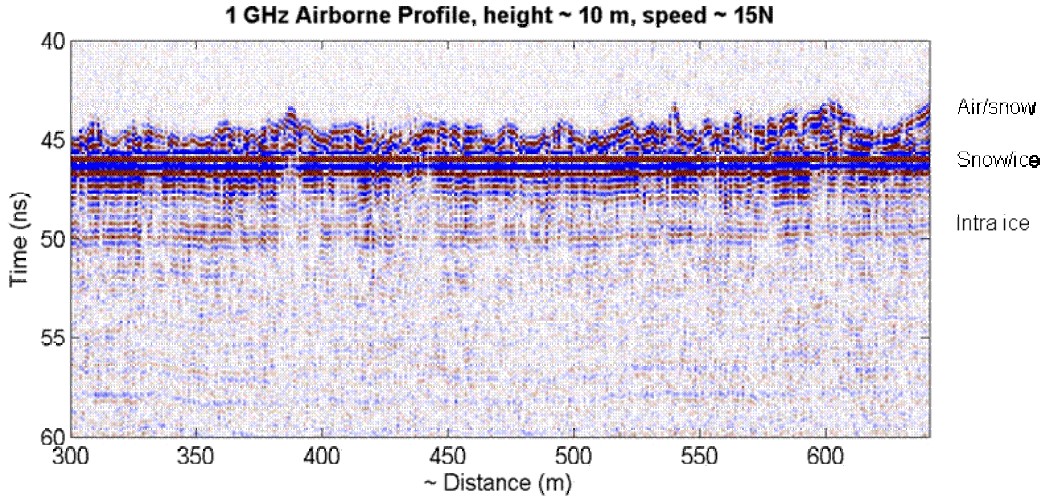

Figure 4.9: 1000 GHz airborne profile acquired approximately 1 km seaward along the fjord from the test cells. The data show a clear image of the top of snow, snow/ice interface, internal snow stratigraphy, and reflections from within the ice column. The data were flattened to the snow/ice reflection.

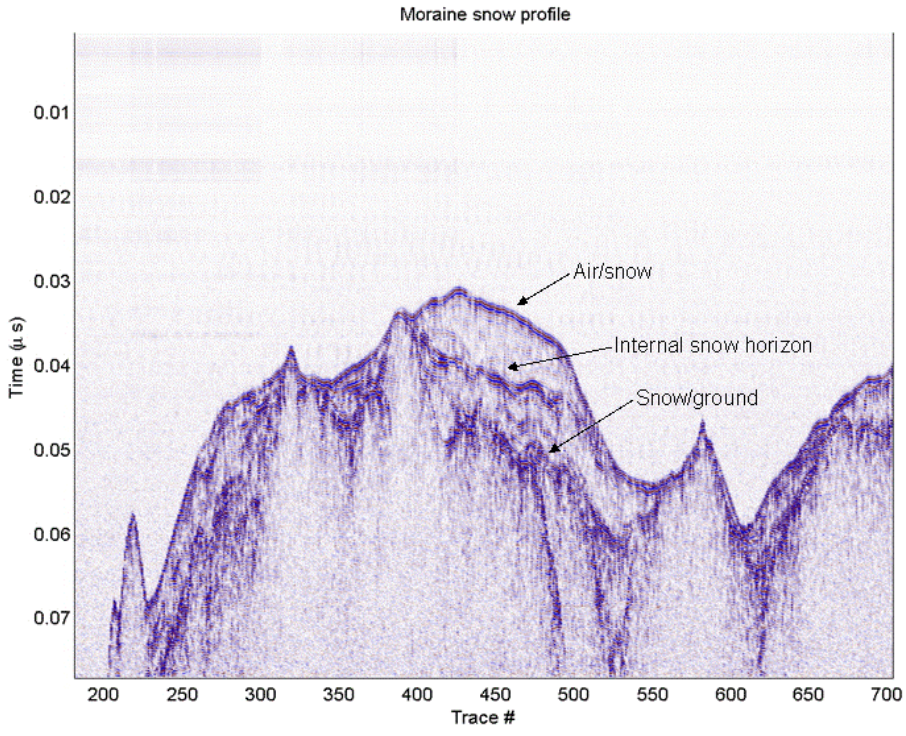

Figure 4.10: 1000 MHz airborne GPR profile showing a clear image of the top of snow, snow stratigraphy, and snow/ground interface.

4.2 Acoustic Measurements

Refer also to Pictures 27 and 28 in Appendix B.

4.2.1 Measured Acoustic Results in Svea Field Tests

During the Svea field experiment, acoustic methods were not possible under in-situ (no surface preparation) conditions due to the presence of upwards of 0.5 m of snow upon the ice surface. We removed the snow from the ice surface along a single transect cutting across the oiled skirt (clean ice under the outside section of trench and oiled ice under the section of trench inside the skirt) and poured approximately 1.0 cm of sea water upon the sea ice to image through the ice. Fig. 4.11A and Appendix B photos.

To confirm the ability to acoustically image through sea ice, we used a 20-degree beam 50 kHz transducer at 1000-watt power to image the seabed at 14.2 m depth. We placed the transducer on the ice surface with no returned signal. Once we applied a thin layer of water on the ice surface, reflections from the water bottom appear (Figure 4.11B). We confirmed the reflection character and water depth with the transducer placed directly on a water surface at the dive hole. We then collected a 50 kHz profile along the ice surface both inside and outside the skirt (Figure 4.12). Along this profile, we observe water bottom reflections near the center of the skirt and outside the skirt, but within approximately 3 m of the skirt boundary the water bottom reflections do not appear. We are unclear as to why the reflections are not visible at these locations because ice surface conditions appeared uniform. The diminished reflection character near the skirt boundary may be due to altered surface ice conditions when the skirt was installed (e.g. local flooding on either side of the chainsaw slot). We observe a consistent reflection from ice bottom depths across the length of the profile.

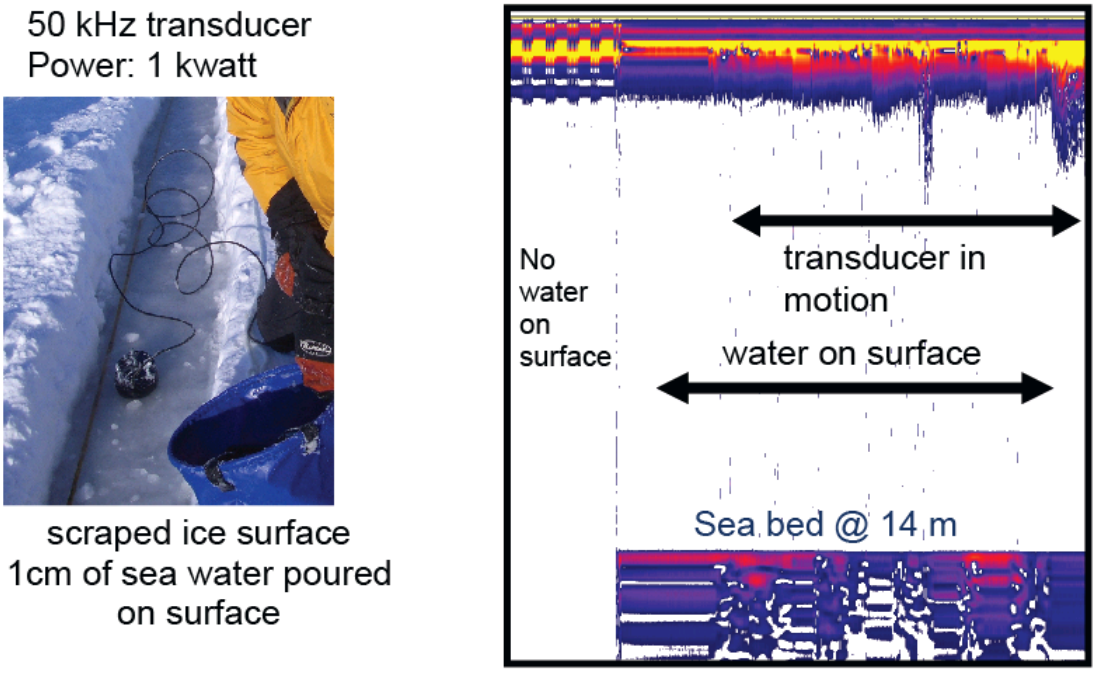

Figure 4.11: A) Photo of acoustic transducer on the ice surface. B) Reflection section from the transducer placed on the ice surface. The left portion of the image shows the response without water to bond the transducer to the ice surface. The right portion of the image shows reflections from below the seabed. The signal in the upper few meters of the figure is from reflections within the ice and immediately below the ice surface. Top arrow shows where we began to move the transducer along the ice surface. Note the changing reflection character both in the upper few meters and along the water bottom reflection package.

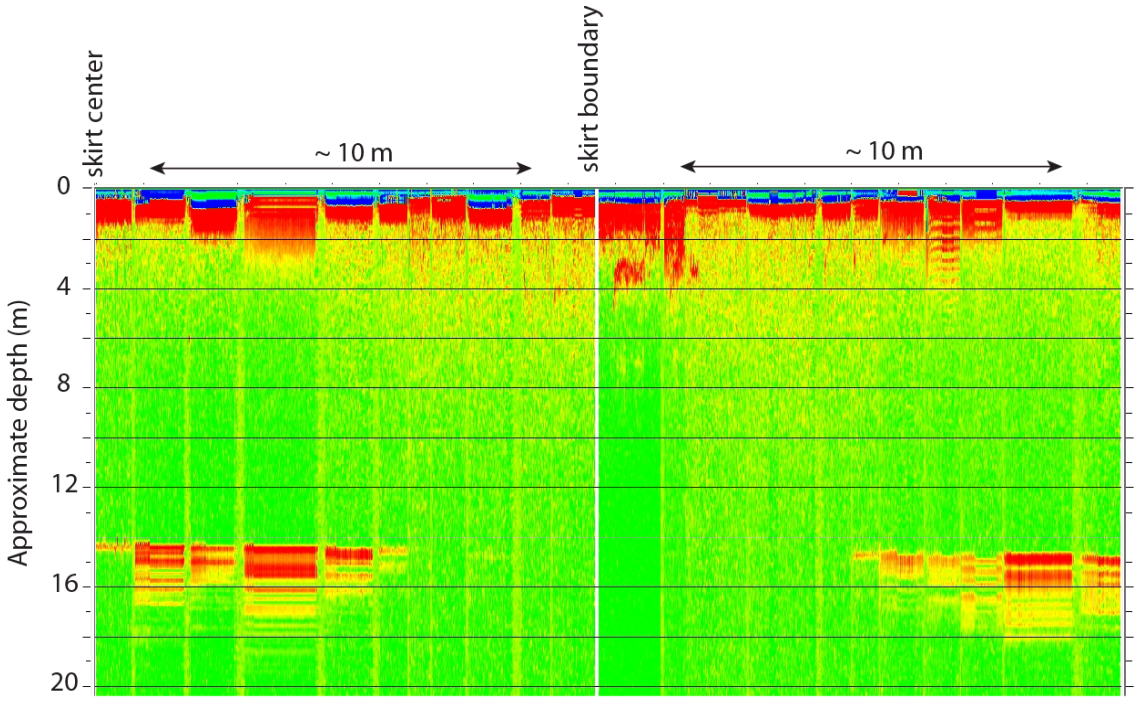

Figure 4.12: Reflection profile from inside the skirt (left) and outside the skirt (right). Soundings were made at static locations for approximately 20 seconds per location; then the transducer was moved approximately 0.5 m along the ground surface. Note the loss of water bottom reflection within a few meters of the skirt boundary.

Next, we acquired data using a 200 kHz transducer at 750 watts to image the ice/fluid interface in the upper one-meter. Figure 4.13 shows two static transducer placements where the base of the ice is clearly imaged. Within the skirt, we interpret the ice/oil interface at 82 cm depth, assuming a 3,000 m/s ice velocity. This location is near the center of the skirt along radial line #3. Approximately 6.9 cm below the ice/oil contact (at API 37.8 velocity), a second reflector may represent the base of the oil. Another reflector below this may represent a multiple from the oil/water contact. Dive measurements place oil thicknesses of approximately 4-8 cm for this location. Outside the oil skirt where 50 kHz water bottom reflections appear, we observe an ice/water contact (Figure 4.13) at a lower amplitude compared to the reflection at the base of the ice within the skirt. This contact appears at 69 cm depth, consistent with measured ice thicknesses. The lower amplitude response is also consistent with the presence on water instead of oil. Coherent energy that follows the ice/water contact is not as strong as observed below the ice/oil contact, again consistent with no interfaces below the ice/water contact. Many other 200 kHz measurements suggest the reflection character of the ice/fluid contact and the oil/water contact changes considerably along the length of the profile. Again, as we approach the skirt boundary with the high frequency transducer, returned signals were significantly diminished.

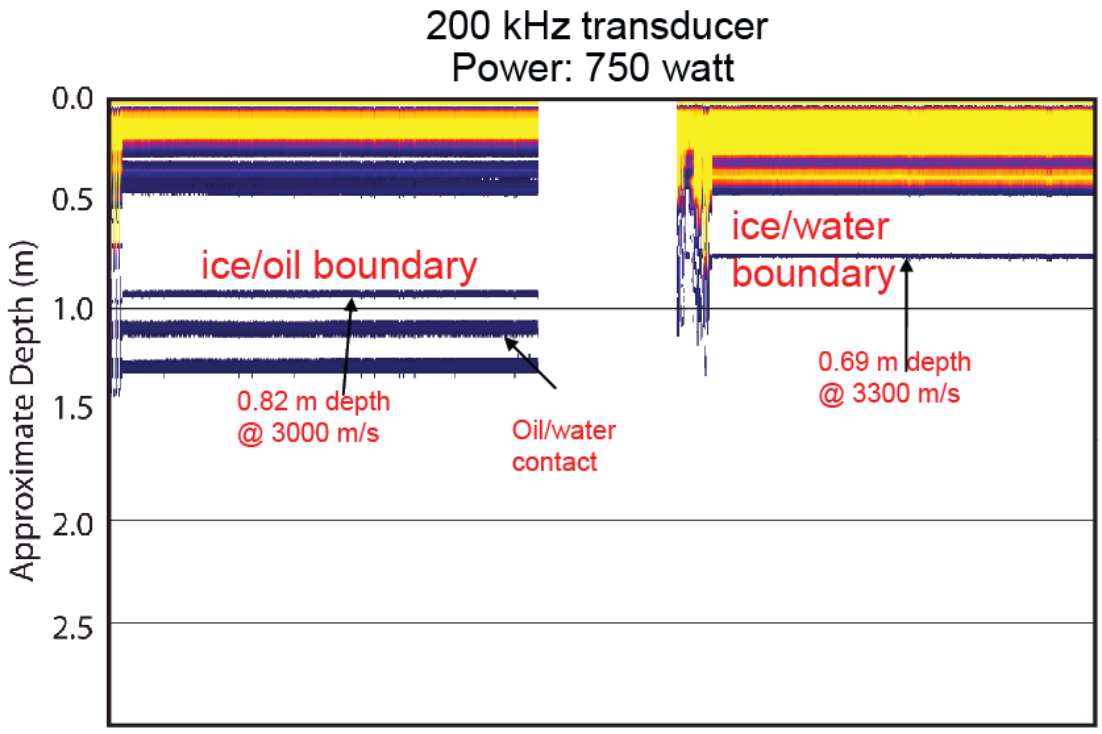

Figure 4.13: Acoustic response from a 200 kHz transducer both within the oil skirt (left) and outside the oil skirt. These locations correspond to where we image water bottom reflections outside the skirt boundary. Note that we observe reflections that we interpret as the ice/oil, oil/water, and ice/water boundaries.

4.3 Oil related data and discussions

These sections contain the data and discussions related to the released oil behavior and properties: migration through the ice sheet and weathering, analytical work on oil and ice samples performed at UNIS/SINTEF, and the in-situ burning operation. Pictures of the different activities are presented in Appendix A.

4.3.1 Mapping of ice properties

Ice thickness at the time of the spill (late March) ranged from 60 to 70 cm compared to an average of 1 to 1.1 m more typically encountered at the end of March. This was reflecting the late freeze-up in the Van Mijen fjord that year. The winter of 2005/06 saw a close to record late freeze-up with a stable ice sheet only beginning to appear at the head of the fjord at the end of January, more than a month later than usual. Appendix C contains a sequence of NASA MODIS satellite images showing the ice edge position in the fjord between March and June 2006. Figure 3.1 shows a satellite image on March 27, the day of spill.

Figure 4.14 (following) documents the salinity variations in the ice during the period of interest.

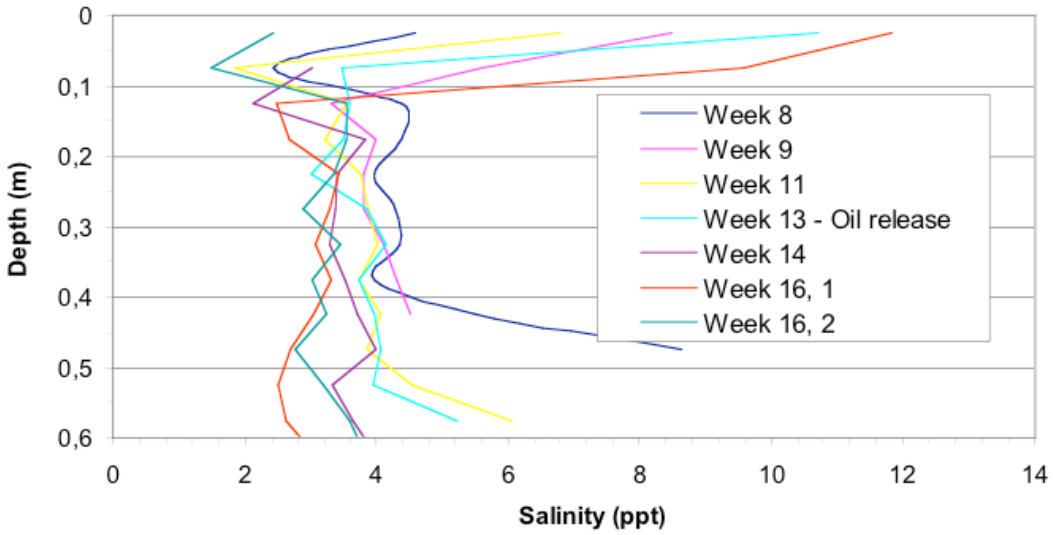

Figure 4.14: Salinity profiles and ice thickness from the experimental site before, under and after the oil release (from Aardahl, 2006)

When seawater freezes, salt is expelled and released as brine in pockets, producing ice with low salinity. The brine pockets move down towards higher temperatures. When temperature in the ice rises during thawing, the brine pockets are gradually turned into brine channels. The salinity profile in sea ice depends on climate conditions, the presence of brine-filled pockets or channels and the presence of an insulating snow layer on top of the ice cover. If sea ice grows in a stable way, the salinity profile will have a C-shape, as seen in Figure 4.14. The top of the sea ice is saltier than the middle part of the ice, because the seawater freezes quicker in the beginning of the ice growth and less salt is expelled. The bottom section is also usual saltier due to brine being expelled in the bottom equilibrium zone, especially during freezing conditions (see profile from week 8 in Figure 4.14).

With time, brine pockets tend slowly to migrate as a result of the temperature gradient within the ice cover. Normally the sense of the temperature gradient is from cold surface to warmer ice lower down and brine pockets migrate downwards by an interesting thermodynamic process. If a brine pocket exists in a temperature gradient, it is energetically favorable for ice to melt at the warmer end of the pocket and refreeze at the colder end. This results in a net migration of the brine pocket towards higher temperatures. The pockets become larger and longer as they migrate since they are passing into progressively warmer surrounding ice and they may coalesce to form major channels of diameter 0.1 to 1 cm diameter. During spring and early summer, at which time the upper and lower surface of the ice can be warmer than the interior, brine slowly becomes expelled to both top and bottom surfaces at the same time (from Sanderson (1988) based on original work by Zubov (1945)).

The variations within the same area could also be significant e.g. due to varying snow cover (see profiles from week 16 in Figure 4.14). Salinity in the top section of the core could also be low due to snow being included in the ice (melting/freezing).

Figures 4.15 and 4.16 show vertical thin sections revealing the ice structure on February 21 and April 20 respectively. Table 4.1 (following) summarizes changes in the crystal structure with depth in terms of the brine pocket height and crystal width (Aardahl, 2006).

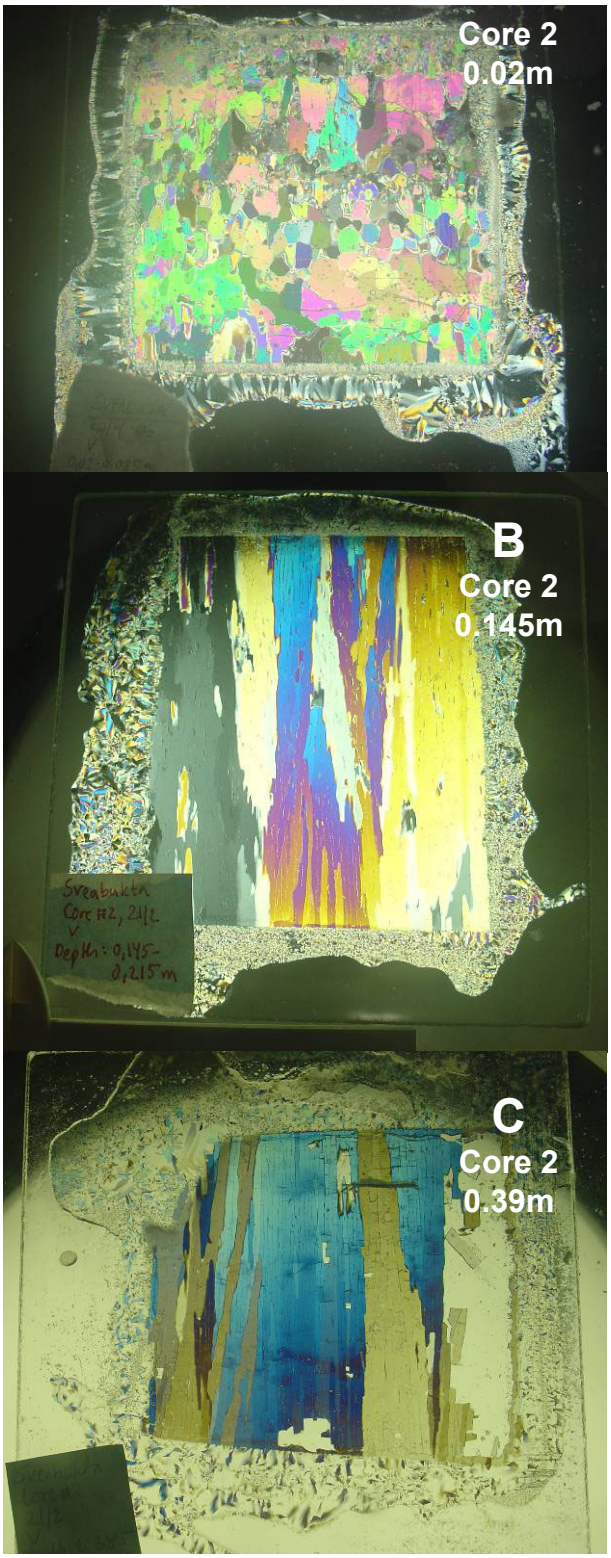

Figure 4.14: Vertical sections images showing the ice structure of the ice core 2 from February 21. A: 0.02 m depth, B: 0.145-0.215 m depth and C: at 0.39 m depth (from Aardahl, 2006).

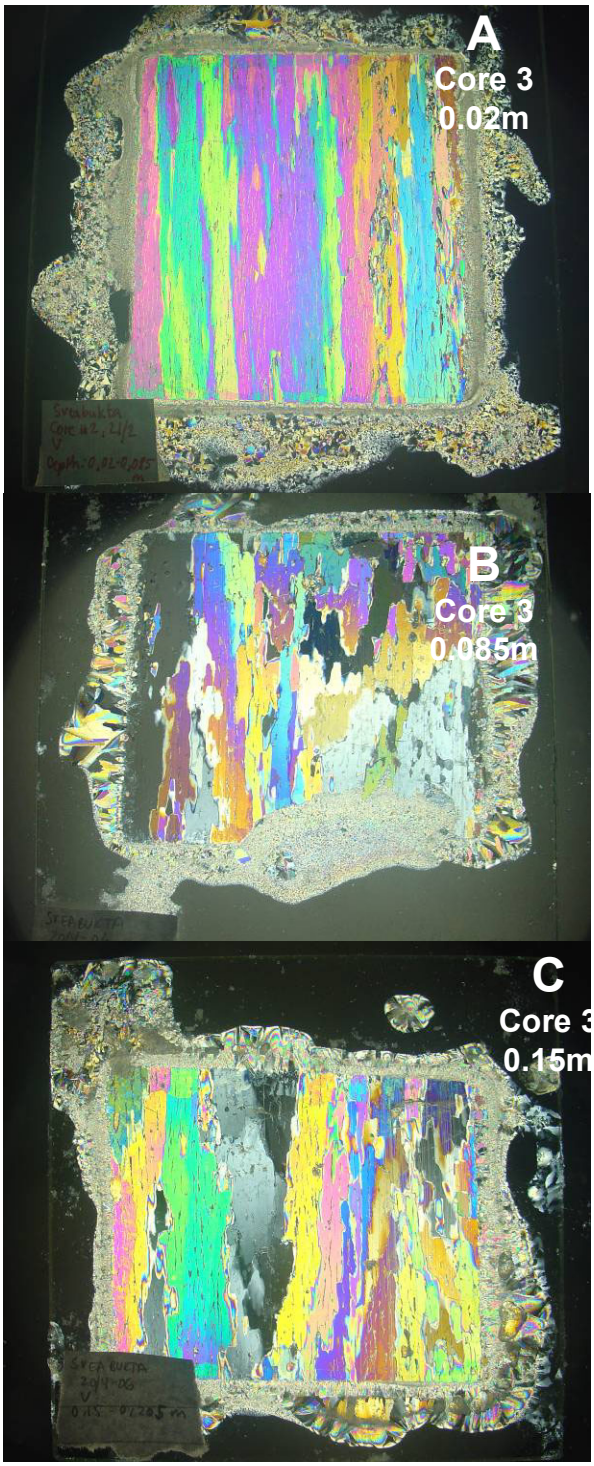

Figure 4.15: Vertical sections images showing the ice structure of the ice core 3 from 20 April. A: 0.02 m depth, B: 0.085 m depth and C: at 0.15 m depth (from Aardahl, 2006).

Table 4.1: Summary of ice crystal structure sampled in week 8 and 16 as a function of depth (from Aardahl, 2006)

Core	Sampling date	Section	Depth [m]	Brine pocket height [m]	Crystal width [m]
2	21.feb	Vertical	0.02	0.0025	0.005
2	21.feb	Vertical	0.085	0.002	0.01
2	21.feb	Vertical	0.145	0.003	0.015
2	21.feb	Vertical	0.26	0.004	0.01
2	21.feb	Vertical	0.33	0.005	0.02
2	21.feb	Vertical	0.385	0.007	0.025
3	20.apr	Vertical	0.02	0.003	0.004
3	20.apr	Vertical	0.085	0.004	0.008
3	20.apr	Vertical	0.015	0.006	0.01

Brine pockets will usually be more numerous and larger for greater depths. This is also confirmed by results from the thin sections of core 2 and 3 (see Table 4.1). When ice is melting, this leads to formation of brine channels in the warm ice, as the brine pockets move down towards lower temperatures. At this time of year with a relatively cold ice core and warm top and bottom, brine can be expelled in both directions up and down. For the core shown, amount, distribution and the size of the brine pockets increase downwards. The amount and size of brine pockets and channels penetrating the crystals, and thus establishing irregularities, increase with increasing temperature of the ice. For that reason, more and bigger pockets could be detected from the latter sampling than from the February cores resulting in thin sections. The average size of the pockets and channels in the cores sampled in February is half the average size of the pockets and channels sampled 8 weeks later at corresponding depths in April 20 (see Table 4.1 above). Not only are there more pockets, but also more cracks indicating a weaker ice.

The Norwegian National Met supplied metrological data for Svea. The data are presented in Figure 4.16 below showing the temperature history for the experimental area. A warm January led to a late freeze-up, followed by conveniently cold weather and solid ice around the oil release date, and then followed by the warmer period opening the brine channels and increasing vertical migration of the oil towards the surface (first observed on April 20 - see Picture 12 in Appendix A).

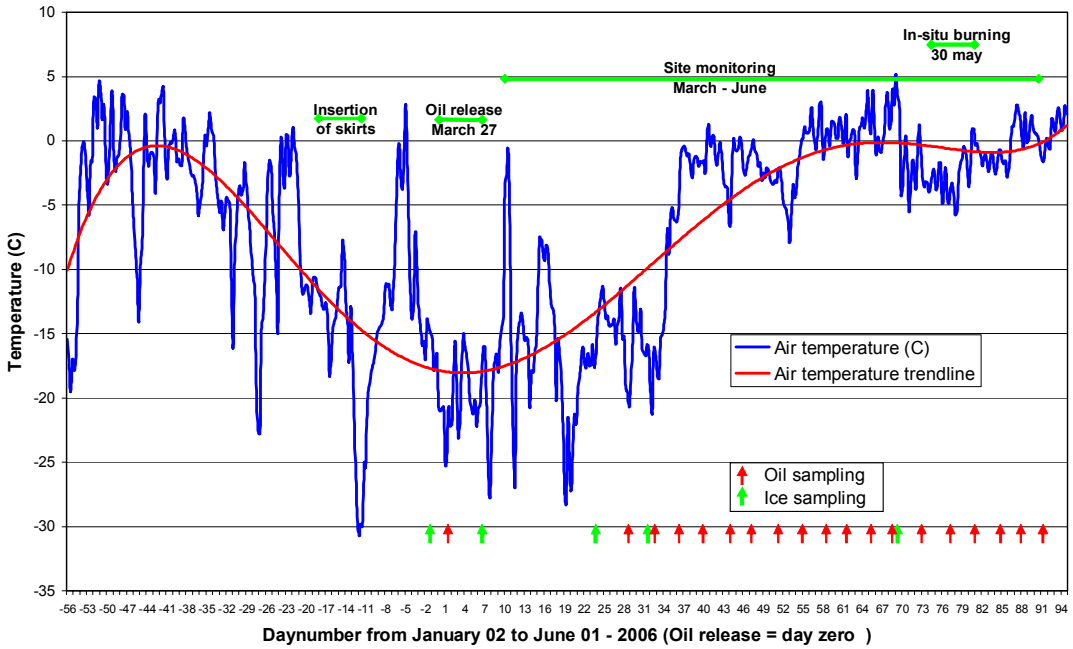

Figure 4.16 Air temperatures f or the experimental site before, under and after the oil release. Important events and sampling events are marked.

4.3.2 Water soluble component in ice cores

Earlier studies have shown that the analyzed components (see Table 3.3) leak out from oil captured in ice and establish significant concentration gradient trough a 1 m ice layer (Faksness and Brandvik 2005 and Faksness et al. 2006). This type of data is important for R&D regarding modeling of environmental impact of oil spills in ice (e.g SINTEF OSCAR model).

Ice cores were collected both outside the skirted areas (reference samples) and inside to study possible migration of water-soluble oil components and oil droplets. A sum of the components given in Table 3.3 is used as a measure for these components (mainly naphtalenes, phenantrenes and dibenzothiophenes). The exact IDs of these components are given in Table 3.3 together with the analytical procedures in the experimental section 3.5.6.

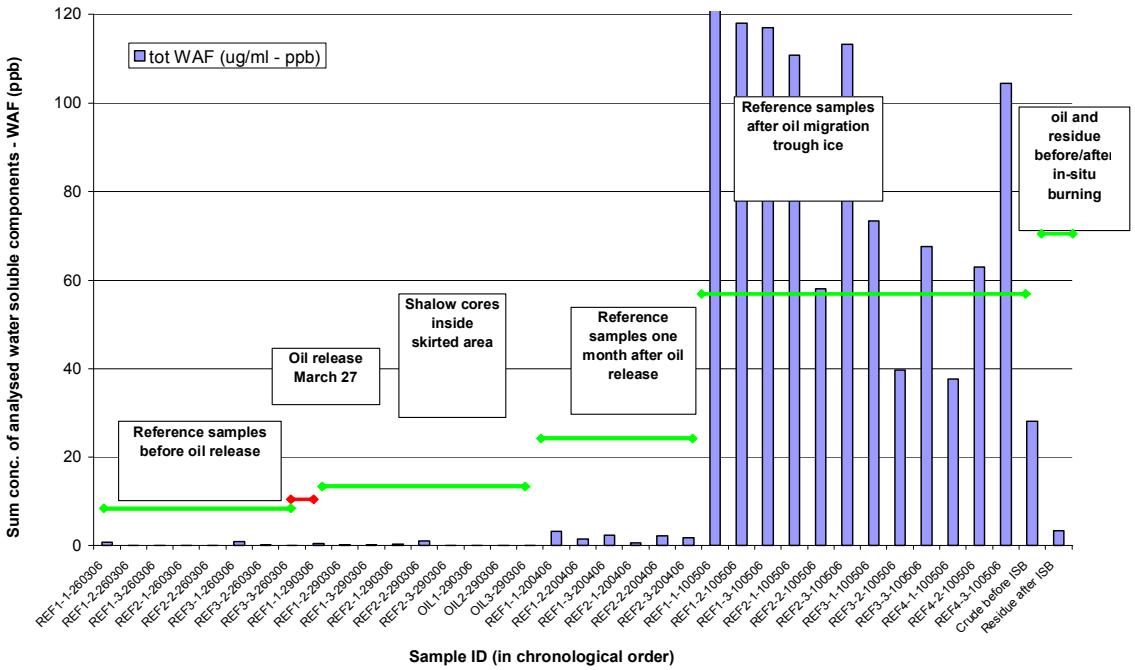

Figure 4.17: Summary concentration of analyzed water-soluble components from all ice cores (reference and inside skirted area). The last part of the sample ID is the sampling date.

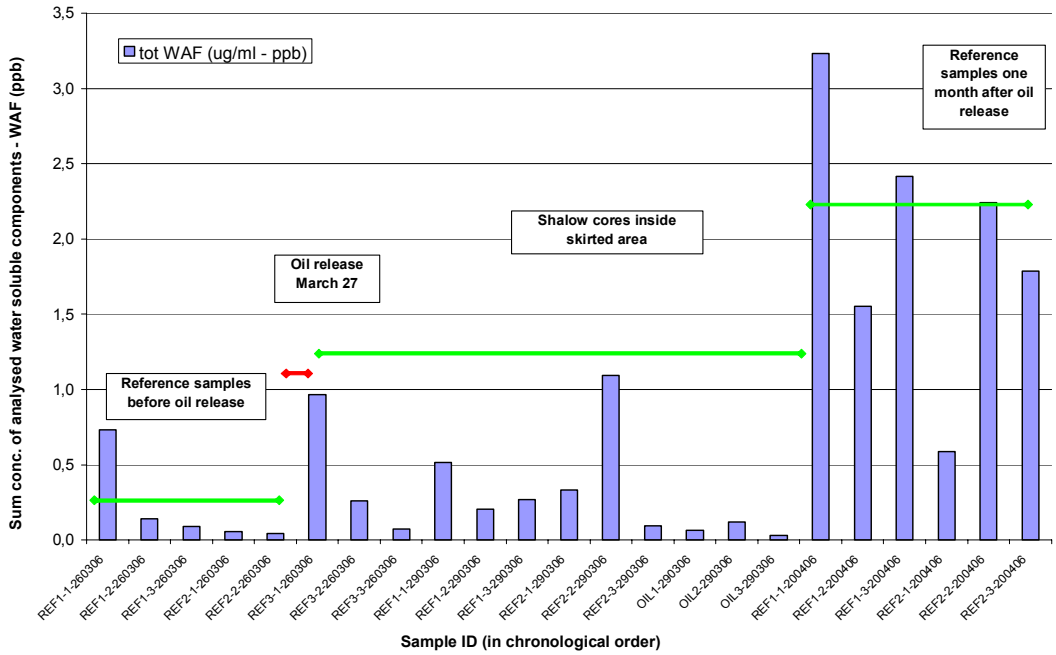

Figure 4.18: Summary concentration of analyzed water-soluble components from selected ice cores containing no bulk oil (reference and inside skirted area). The last part of the sample ID is the sampling date.

The cores used to provide the analysis results in Figure 4.18 and Figure 4.19 were divided in three sections (approx. 3 x 20 cm), numbered REF1-1, 1-2 and 1-3 etc (Figure 3.8). There are some small differences between the three sections of each core. Some of the top sections of the reference cores show increased concentrations (sub ppb), probably due to aerial fall out (e.g. emissions from Svea power plant or snow mobiles). The reference cores sampled after the oil release (March 29) and those collected before the oil release (March 26) showed no significant difference in water-soluble components (see Table 3.3). Also the three shallow cores (20 cm), taken inside the oiled skirted area on March 29, two days after the oil release and analyzed at UNIS/SINTEF, showed oil contents similar to the reference samples (see Figure 4.19).

However, one of the cores taken inside the skirt on March 29 and sent to ETI labs in Houston showed presence of very fine droplets in the brine channels to within 17 cm of the surface. In addition, one of the reference cores taken immediately outside the skirt and also analyzed in Houston showed a band of very fine oil droplets in the skeletal layer (bottom 2.5 cm). See Pictures 10 and 11 in Appendix A and summary of results in Appendix E. These oil droplets were likely generated at the point of flow expansion at the end of the discharge pipe. A small portion of these droplets in the smallest size range could have remained suspended to be carried outside the test area within the 48 hours that elapsed between the spill and coring.

On April 20 the oil was visually detected on the ice surface (under the snow inside the skirted area, see Picture 12 in Appendix A). The levels of oil soluble component in the reference samples taken outside the skirted area were increased by a factor of approximately 2. Since no bulk oil was detected in these cores, (only water-soluble components were detected) these results show a significant increase in water-soluble components due to migration through the porous first year ice (see Figure Figure 4.18).

The rate of oil migration through the ice was monitored by visual inspection of the ice and by analyzing the oil content in ice cores.

The rate of oil observed in this experiment on Svalbard (Figure 4.20 below) makes an interesting comparison with a previous oil-under-ice experiment in the Canadian Beaufort Sea carried out in 1979/80 (Dickins et al., 1981). Oil from the first spill in that experiment rose through a similar ice thickness (60 to 70 cm) to reach 100% exposure in approximately 40 days from first appearance under the snow, results very similar to the timing of oil appearance documented at Svea.

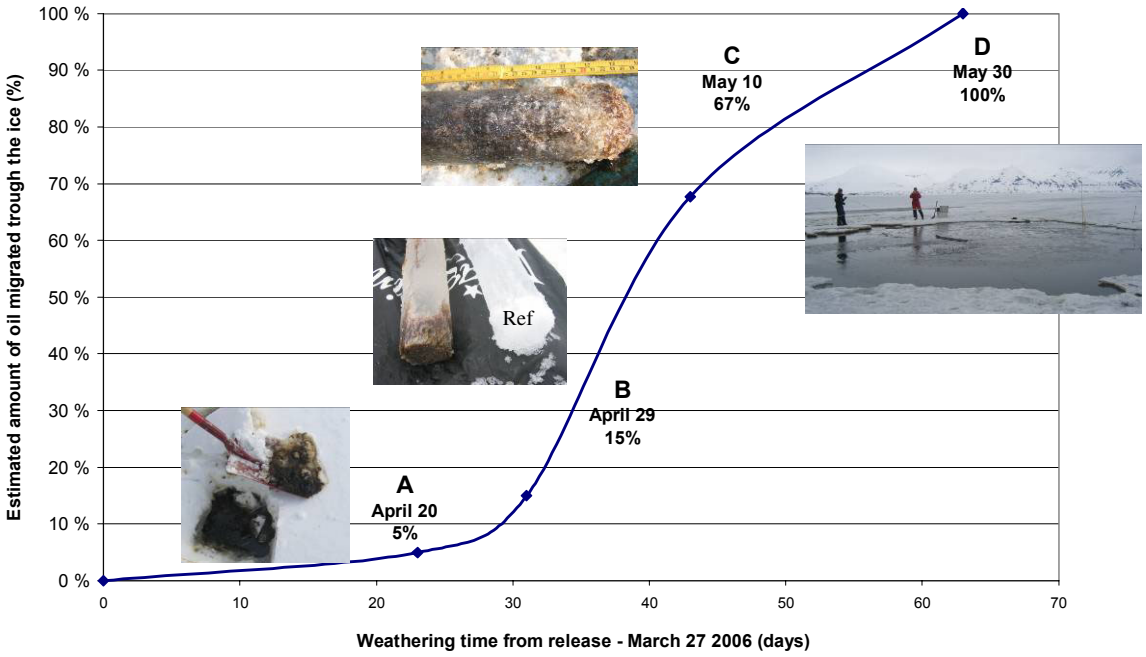

Figure 4.19: Estimated amount of oil penetrated through the brine channels in the ice and available on the ice surface. Inserted pictures show oil on top of snow (A), cores drilled through the ice to quantify oil captured in the ice (B + C) and the final melt pool (D).

4.3.3 Oil distribution and oil film thickness

The average film thickness based on the size of the skirted area (100 m^2) and the amount of oil released (3,400 l) was calculated as 3.5 cm. However, natural variability in the ice thickness (±5+ cm on average) was expected to create deeper pockets of oil in some areas. The field data measured on-site by the divers are given as blue numbers in Figure 4.20 and the interpolated thicknesses in black numbers. The average difference between interpolated and measured data is < 5%. The "bi-modal distribution" of the oil film in two areas with significantly higher thickness than the rest of the area (14 to 18 cm measured), might be explained by the position of the release pipe and maybe changing tidal currents during the oil release.

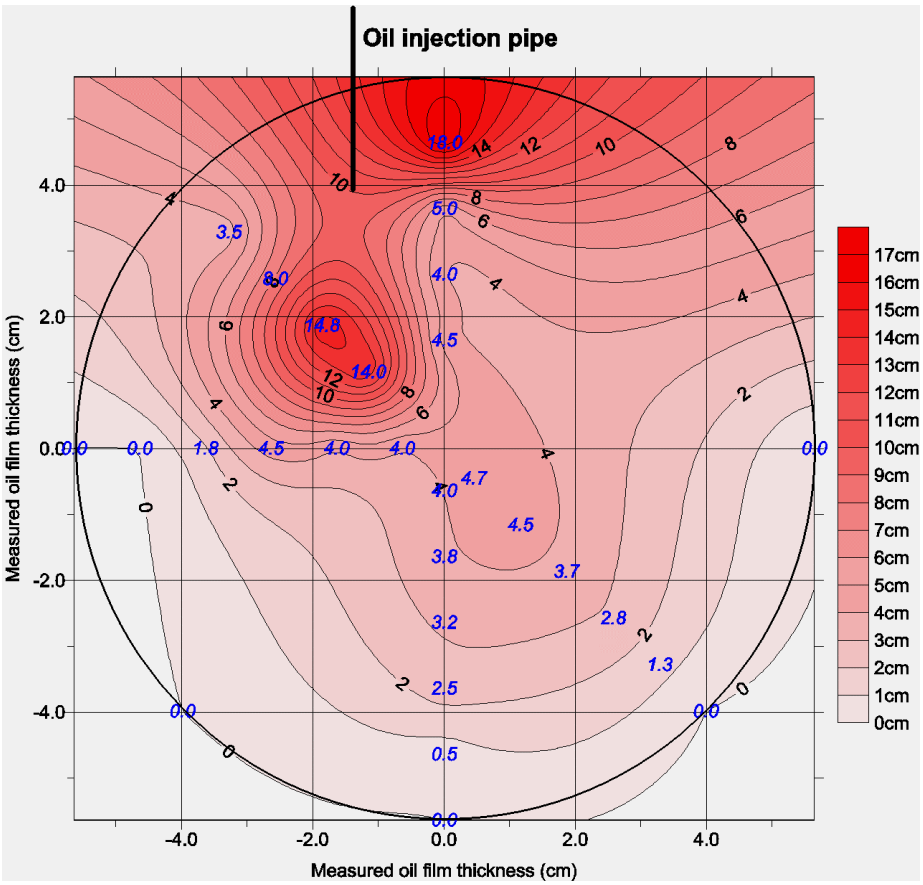

Figure 4.20: Under-ice oil film thickness. Field data acquired by divers are given in blue italics, interpolated curves (Krieging algorithm) and estimated thicknesses in black numbers (cm). The circle represents the 100m^2 skirted area. No significant amount of oil was spilt outside this circle.

The volume of the interpolated surface describing oil thickness (inside the circle) is calculated to 4030 liters of oil. This corresponds to an average film thickness of 4.1 cm, approximately 20% higher that the released amount of oil. This is probably due to an overestimation of the thick areas based on a limited number of field measurements in the thick areas (blue numbers in Figure 4.21).

4.3.4 Oil weathering

After migrating through the ice and appearing on the ice surface after approximately 23 days, the oil was sampled approximately every second day. Evaporative loss (weight %) was measured on these samples. The evaporative loss in the surface samples was variable but relatively stable in the 30 – 35% range. Towards the end of the experiment the evaporative loss of the bulk surface oil drops from 36 to 27% (see *Figure 4.21*). This shift is most likely caused by fresh oil still being released from the ice and reducing the average evaporative loss of the bulk oil on the surface.

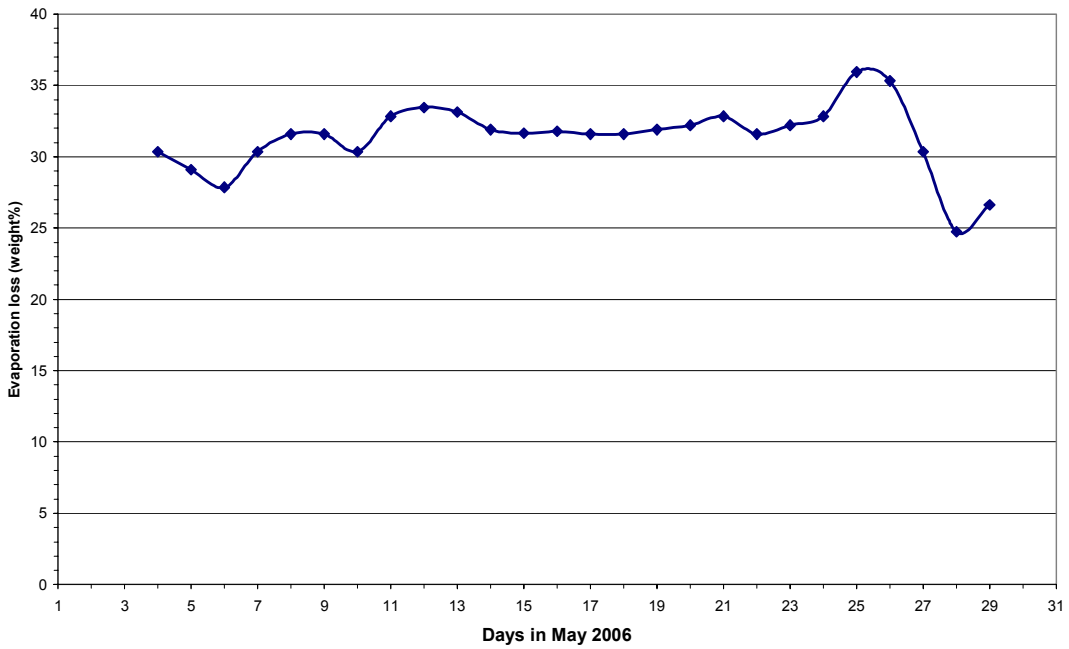

Figure 4.21: Evaporative loss for oil surfacing in the oil melt pool on the ice after April 20. until May 30. 2006. The samples of the surface oil in the melt pool were analysed by GC and selective chromatograms are shown in Figure 4.23.

Chromatogram A shows the crude oil as released on March 27. This sample has all the light components intact. The second chromatogram in B shows the weathered oil on May 30 before the in-situ burning. This oil sample is clearly missing light components up to C_9 and corresponds almost to a 200ºC+ residue (32% loss). An evaporative loss of 27% for an oil spill on the ice surface at low temperatures could seem high, but the effect of solar heat gain must be considered. With 24 hours of sunlight from April 20 on, the sun warmed the surface oil to between +2 and +10ºC. In addition, the relatively low film thickness would also promote efficient evaporation when the oil began to surface.

Oil appearing initially was exposed to evaporative weathering conditions for over one month (April 20 to May 30.). The estimated evaporative loss of 27% on May 30 was based on measurements of density and gas chromatographic analysis. The evaporative loss was correlated against density by using the SINTEF oil-weathering model. The evaporative loss was also controlled by comparing gas chromatogram of the weathered oil on May 30 with a gas chromatogram from similar residues prepared in the laboratory. Pictures showing the oil in the melt pool are shown in Appendix A (Picture 13 to Picture 15).

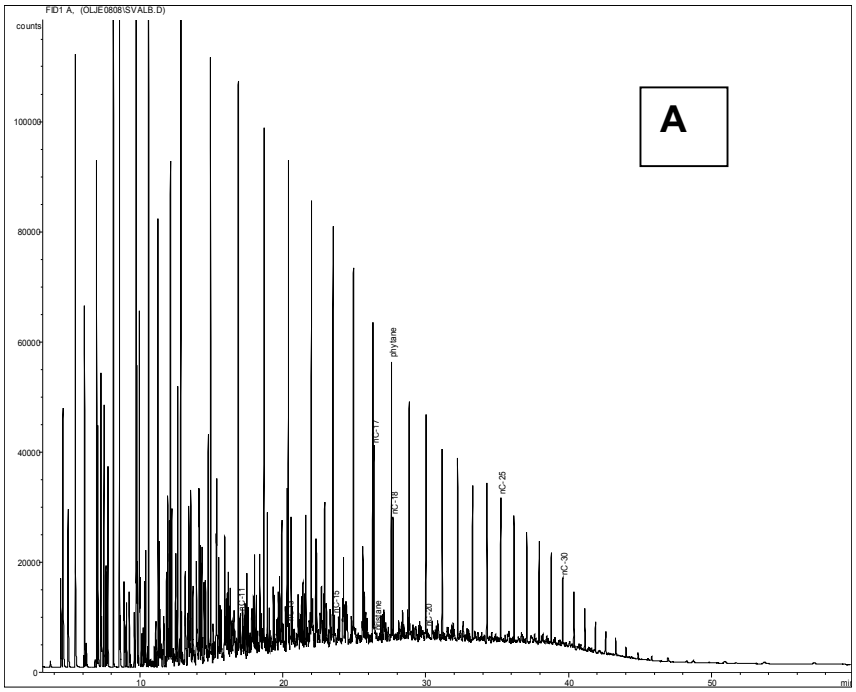
FID1 A, (OLJE0808\SVALB.D)
counts
A
nC-17
pristane
phytane
nC-18
nC-25
nC-30
nC-20
nC-15
nC-11
0
20000
40000
60000
80000
100000
10
20
30
40
50

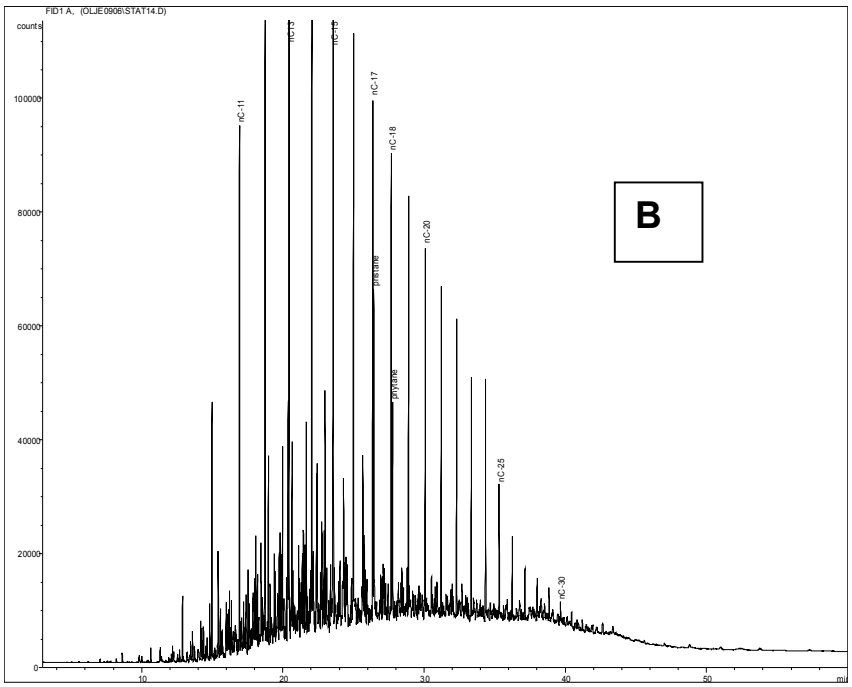
FID1 A, (OLJE0906\STAT14.D)
counts
B
nC-11
nC-17
nC-18
nC-20
pristane
phytane
nC-25
nC-30
0
20000
40000
60000
80000
100000
10
20
30
40
50

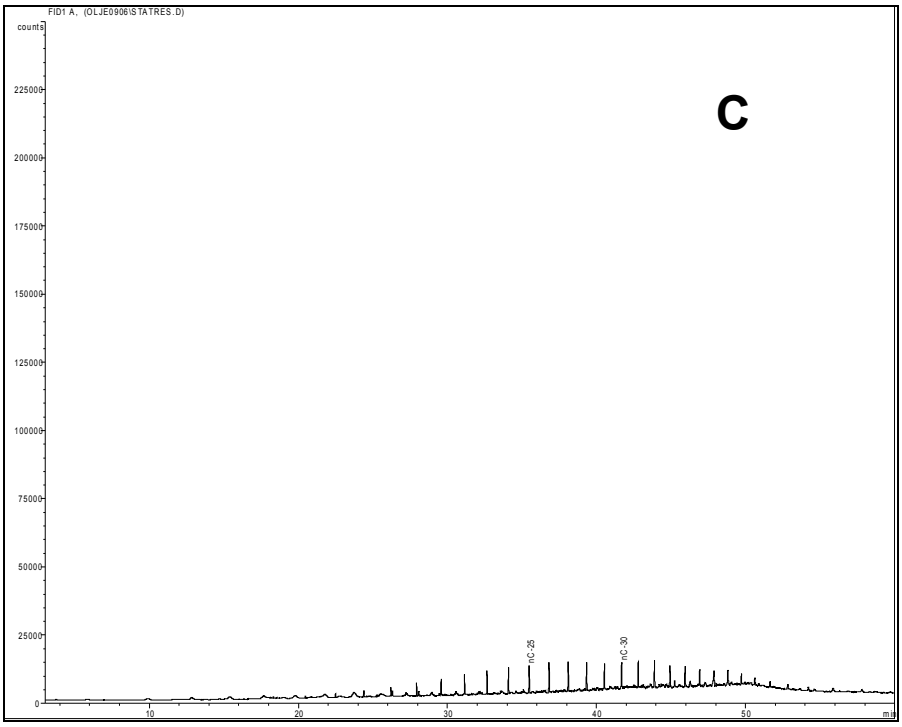

Figure 4.22: Gas chromatograms A: released fresh crude. B: weathered oil before in-situ burning May 30. C: residue after in-situ burning.

Water content was also measured in the samples taken approximately every second day after the oil started to appear on the ice surface. The water content in the samples varied up to 7%, but a single sample showed 19% (see Figure 4.24). There was very little wave energy available in the melt pool so conditions were not very favorable for formation of water-in-oil formation. A water content of a few percent (0-5%) is as expected under such conditions. The outlier (19%) is probably caused by poor sampling, where water is sampled together with the surface oil.

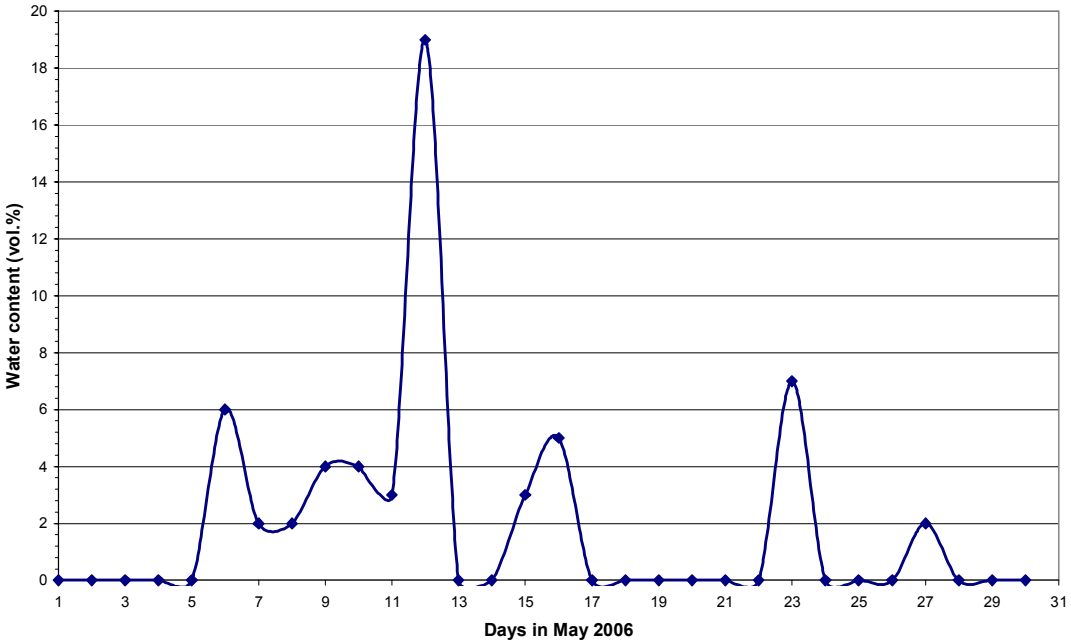

Figure 4.24: Water content (vol.%) of the oil surfacing in the oil melt pool on the ice after April 20. until May 30. 2006.

4.3.5 In-situ burning

In-situ burning of the surface oil was carried out on May 30 in very favorable weather conditions: 4ºC, 2 m/s wind and with a high cloud base.

Pictures from the in-situ burning operation are given in Appendix A (see Picture 16 to Picture 21). The most important in-situ burning results are presented in table 4.2. The last chromatogram C in
Figure 4.22 represents the burning residue, and demonstrates that most of the light components were consumed in the burn (up to C_{20}).

Table 4.2 summarizes parameters measured in documenting the in-situ burn.

Table 4.2: In-situ burning summary

In-situ Burning Summary	
Oil Type	Statfjord crude
Initial oil volume (liters)	3400
Evaporative loss (vol.%)	27
Weathered oil volume (liters)	2482
Oil film thickness (mm)	35
Oil film area (m^2)	69
Burning time (min)	11
Terminal oil thickness (mm)	1
Residue (liters)	106
Density of residue (g/ml)	0.9412
Burning efficiency (%)	96 %
Burning rate (mm/min)	3,1
Burning rate (liters/min)	216

The oil film thickness shown Table 4.2 was measured on the oil layer in the melt pool on site. During the eleven minute burn, the oil spread out and filled the approximate 100 m^2 melt pool. The burning effectiveness is calculated by comparing the actual oil volume burned (weathered oil - residue) with the weathered oil volume. Further details are provided in Daniloff (2006).

The combustion process appeared visually to be starved, and created a dark smoke plume. The smoke plume could be followed by eye for approximate 500 meters before it diluted completely and could not be distinguished from the background.

5. References

Aardahl, I.B. 2006. "Salinity and Thin sections from First-year Sea Ice in the van Mijenfjord Spring 2006". Student paper in AT-208 Physical Properties of Materials. The University Center at Svalbard – UNIS, Longyearbyen, Norway.

Batzle, M. and Wang, Z. 1992. Seismic Properties of Pore Fluids. *Geophysics*. 57 (11), p. 1396-1408.

Bech, C., Sveum, P., and I.A. Buist. 1993. The Effect of Wind, Ice and Waves on the In-Situ Burning of Emulsions and Aged Oils. Proceedings 16th Arctic Marine Oil Spill Program (AMOP) Technical Seminar, Calgary, Alberta, pp 735-748.

Bradford, J.H. July 2005. Task 4 Technical Note: GPR Software Development**.** Report by DF Dickins Associates Ltd. and Boise State University to the Minerals Management Service, Herndon, VA (Contract No. 0105PO39137).

Bradford J.H., Liberty L.M, and Dickins D.F. 2005. Oil Exploration at less than 2 M Depth: Instantaneous Attribute Analysis of Ground-Penetrating Radar Data for Detection of Crude Oil Under Sea Ice. SEG Technical Program Expanded Abstracts, pp. 1113-1116.

Brandvik, P.J., Faksness L-G, Dickins D.F. and Bradford J.H. Weathering of Oil Spills Under Arctic Conditions - Field Experiments with Different Ice Conditions Followed by In-Situ Burning. Presentation at NATO/CCMS third workshop on Oil Spill Response, Halifax, Nova Scotia, October 2006.

Brandvik, P.J., Singsaas, I., and P.S. Daling. 2004. Oil Spill R&D in Norwegian Arctic Waters with Special Focus on Large-scale Oil Weathering Experiments. Paper presented at the Inter Spill Conference, Trondheim, Norway.

Brown, H.M. and R.H. Goodman. 1986. In Situ Burning of Oil in Experimental Ice Leads. Environmental Studies Revolving Funds Report 064. National Energy Board, Calgary.

Buist, I.A. and D.F. Dickins. 1987. Experimental Spills of Crude Oil in Pack Ice. Proceedings of the 1987 Oil Spill Conference, April 6-9, Baltimore, Maryland. American Petroleum Institute, Washington, D.C. pp 373-382.

Comfort, G., Roots, T., Chabot, L. and F. Abbott. 1983. Oil Behaviour Under Multi-year Ice at Griper Bay, NWT. Proceedings 6th Arctic and Marine Oil Spill Program Technical Seminar, Environment Canada, Ottawa.

Daniloff, R. 2006. In-situ Burning of Oil Spills". MSc thesis at the Norwegian University of Technology and the University Center at Svalbard (UNIS), Norway.

Dickins, D.F. July 2005. Preliminary Project Plan: 2006 Field Spill to test Oil-in-Ice Detection Technologies. Report submitted to the Minerals Management Service, Herndon, VA.

Dickins, D.F. 2004. Advancing Oil Spill Response in Ice Covered Areas. Report submitted to the Prince William Sound Oil Spill Recovery Institute and US Arctic Research Commission, Cordova Alaska and Washington DC.

Dickins, D.F. October 2000. Detection and Tracking of Oil Under Ice. Final report submitted by DF Dickins Associates Ltd. to Minerals Management Service, Herndon VA.

Dickins, D., Liberty L., Hirst W., Bradford J., Jones V., Zabilansky L., G. Gibson G., and J. Lane. 2005. New and Innovative Equipment and Technologies for the Remote Sensing and Surveillance of Oil in and Under Ice. Proceedings 28 th Arctic and Marine Oilspill Program Technical Seminar, Calgary, June 2005. (MMS Contract 1435-01-04-36285)

Dickins, D.F. and J. Bradford. July 2005. Field Testing GPR over a Variety of Sea Ice Conditions at Prudhoe Bay, Alaska April 18-20, 2005. Field report submitted by DF Dickins Associates Ltd. and Boise State University to the Minerals Management Service, Herndon, VA (Contract No. 0105PO39137).

Dickins, D.F., Buist, I.A., and W.M. Pistruzak. 1981. Dome Petroleum's Study of Oil and Gas Under Sea Ice. Proceedings International Oil Spill Conference, American Petroleum Institute, Wash. D.C., pp 183-189.

Faksness, L-G., Brandvik, P.J. and M. Reed. 2006. Chemical Characterization of Water-soluble Components from Arctic Marine Oil Spills – a combined laboratory and field study. Paper presented at the 9th International Marine Environmental Modelling Seminar (IMEMS), Rio de Janeiro.

Faksness, L-G., Grini, P.G., and P.S. Daling. 2004. "Partitioning of Semi-soluble Organic Compounds between the Water Phase and Oil Droplets in Produced Water". *Marine Pollution Bulletin*, 48, pp 731-742.

Faksness, L-G., and P.J. Brandvik. 2005. Dissolution of Water Soluble Components from Oil Spills Encapsulated in Ice. Proceedings 28th Arctic and Marine Oilspill Program Technical Seminar (AMOP), pp 59-73.

Guénette, C.C. and R. Wighus. 1996. In Situ Burning of Crude Oil and Emulsions in Broken Ice. Proceedings of the 19th AMOP Technical Seminar. Calgary, AB. pp 895 - 906.

Jones, H.W., and Kwan, H.W., 1982, The Detection Of Oil Spills Under Arctic Ice by Ultrasound. Proceedings of the 5th Arctic and Marine Oilspill Program Technical Seminar, Environt Canada, Ottawa, p. 391-411.

Jones, H.W., Kwan, H.W., Hayman, T., and Yeatman, E.M. 1986. The Detection of Liquids and Viscoelastic Substances Trapped Under Solid Surfaces. *Journal of Acoustical Society of America*, 79(1), p. 84-90.

Liberty L.M., Bradford, J.H., Dickins, D.F. and P.J. Brandvik. 2007. Ultrasonic Imaging Through Sea Ice. Submitted for publication in Geophysical Research Letters (GRL).

Liberty L.M., Bradford J.H., Brosten T.R., and Dickins D.F. 2006. Acoustic Imaging Through Sea Ice. Proceedings Society of Exploration Geophysicts (SEG) Conference 2006.

Løset, S., Singsaas, I., Sveum, P., Brandvik, P.J., and H. Jensen. 1994. Oljevern i nordlige og arktiske farvann (ONA) - Status: Volum I and II. STF60 F94087.

NORCOR Engineering and Research Ltd. 1975. The Interaction of Crude Oil with Arctic Sea Ice. Beaufort Sea Project Technical Report No. 27, Canada Department of the Environment, Victoria, British Columbia.

Payne, J.R., Daniel, G., McNabb J.R. and J.R. Clayton. 1991. Oil Weathering Behavior in Arctic Environments. Proceedings Pro-Mare Symposium on Polar Marine Ecology,Trondheim.

Sanderson, T.J. 1988. *Ice Mechanics: Risks to Offshore Structures.* Graham and Totman, London.

Shell Oil Company, Sohio Alaska Petroleum Company, Exxon Company, U.S.A., Amoco Production Company. 1983. Oil Spill Response in the Arctic - Part 2: Field Demonstrations in Broken Ice., Prepared by A. Allen for Shell Oil, Sohio Alaska, Exxon, and Amoco. Anchorage, Alaska.

Sheriff, R.E. 2002. *Encyclopedic Dictionary of Applied Geophysics, Fourth Edition*. Society of Exploration Geophysicists, 323 p.

Singsaas, I., P. Brandvik, P. Daling, M. Reed and A. Lewis. 1994. Fate and Behavior of Oils Spilled in the Presence of Ice. Proceedings of the 17th AMOP Technical Seminar, June 8-10, Vancouver, British Columbia, pp 355-370.

SL Ross Environmental Research Ltd., DF Dickins Associates Ltd. and Alaska Clean Seas. 2003. Tests to Determine the Limits of In Situ Burning of Thin Oil Slicks in Broken Ice. Report prepared for the US Minerals Management Service and ExxonMobil.

SL Ross Environmental Research Ltd. and DF Dickins Associates Ltd. 1987. Field Research Spills to Investigate the Physical and Chemical Fate of Oil in Pack Ice. Environmental Studies Revolving Funds Report No. 062. 95 p.

Smith, N.K. and A. Diaz. 1987. In-place Burning of Crude Oils in Broken Ice. Proceedings of the 1987 Oil Spill Conference, April 6-9, Baltimore, Maryland. American Petroleum Institute, Washington, D.C. pp 383-387.

Vefsmo S., Jensen, H., Singsaas, I. and C. Guenette. 1996. Oil Spill Response in Ice Infested waters. SINTEF report STF22 F96202. SINTEF Trondheim. Norway.

Vefsnmo,S. and B.O. Johannessen. 1994. Experimental Oil Spill in the Barents Sea: Drift and Spread of Oil in Broken Ice. Proceedings 17th Arctic and Marine Oil Spill Program Technical Seminar, Vancouver, BC.

Xie, Y. and Farmer, D.M., 1994, Seismic acoustic sensing of sea ice wave mechanical properties, *Journal of Geophysical Research*, Vol. 99, No. C4, p. 7771-7786 (93JC03483).

Zubov, N.N. 1945. Arctic Ice. Izdatel'stvo Glavsermorputi, Moscow. English translation by US Navy Oceanographic Office/American Meteorological Society.

Appendix A – Photo Album: Oil Spill Execution and Documentation

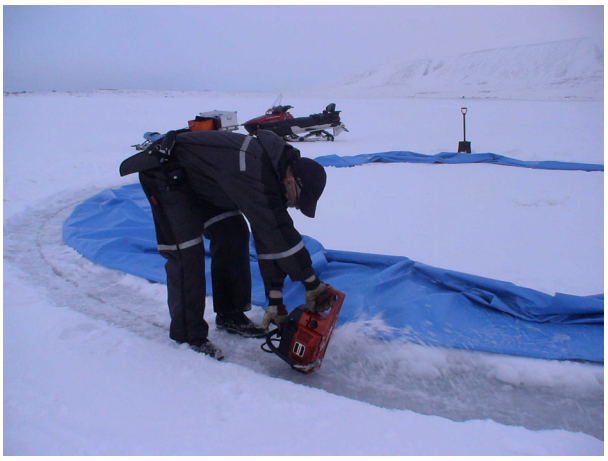

Picture 1: *Cutting in the oil skirts to prevent oil from spreading under the ice, February 2006*

Picture 2: *Completed skirt installation, February 2006*

Picture 3: *Pumping oil from drums through flexible pipe inserted 1 m inside skirt through a sloped hole drilled 2 m outside, May 27. 2006*

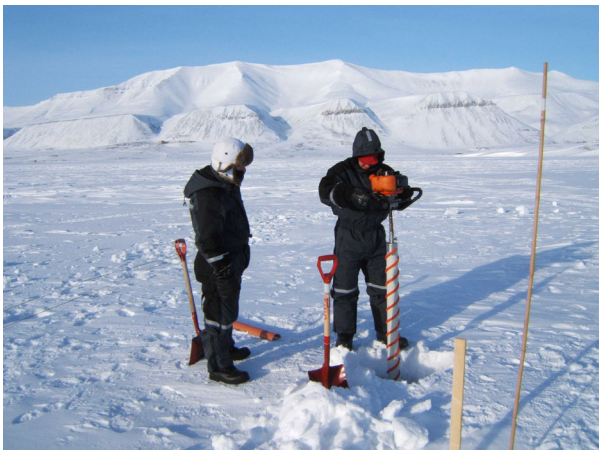

Picture 4: *Taking a reference ice core outside the skirted area before the oil release, May 26. 2006*

Picture 5: *Extracting an ice block while cutting a dive hole just outside the skirt, May 26. 2006*

Picture 6: *Ice block total thickness 62 cm floating on its side in the dive hole showing transitions in ice structure from random orientation to columnar at ~15 cm and to clear slower growing ice with less air intrusions) at a depth of 44 cm*

Picture 7: *Diving operations to monitor the oil layer thickness under the ice, May 28.2006.*

Picture 8: *SINTEF prototype under-ice oil thickness sampler used to measure oil film thickness under ice, May 26.2006.*

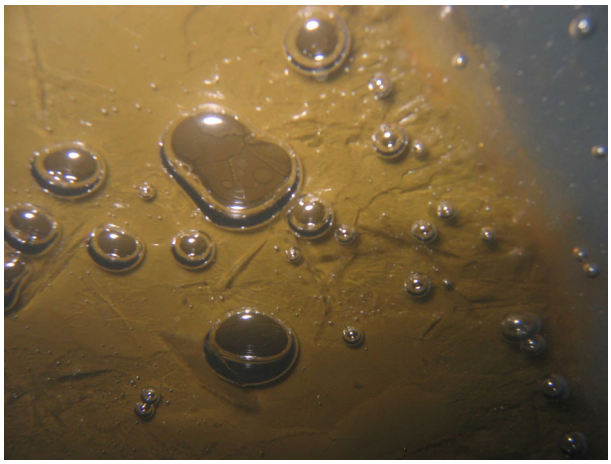

Picture 9: *View of oil layer under the ice showing evidence of large, new ice crystals floating within the oil*

Picture 10: Close-up showing small oil drops (0.2 to 1 mm) in the bottom 2.5 cm of a core taken outside the oil skirt on March 29, 48 hours post-spill (Ref.3 location in Figure 3.4)

Picture 11: Close-up of oil in brine channels within the lower 8 cm section of a 23 cm core taken from Location 3 inside the oiled area on March 29 (Figure 3.4)

Picture 12: First visual contact with oil on, under snow, top of ice. April 10. 2006.

Picture 13: Oil in the melt pool on the ice, April 20. 2006

Picture 14: Oil in the melt pool on the ice, May 10. 2006.

Picture 15: Oil in the melt pool on the ice, May 30. 2006.

Picture 16: Ignition of oil with handheld igniter (a slab of gelled n-hexane on the oil and butane torch). May 30. 2006.

Picture 17: In-situ burn 5 minutes after ignition, May 30. 2006.

Picture 18: In-situ burning at the end of the burn, May 30. 2006.

Picture 19: In-situ residue after 2 hours of cooling. Semi-solid, thickness 1 mm. May 30. 2006

Picture 20: Collection of residue after burn termination, May 30. 2006

Picture 21: Melt pool after burn and treatment of oil adsorbent. May 30. 2006

Appendix B – Photo Album: Remote Sensing Activities

Picture 22: Radar traverse along survey grid line

Picture 23: Close-up of the ground penetrating radar antenna

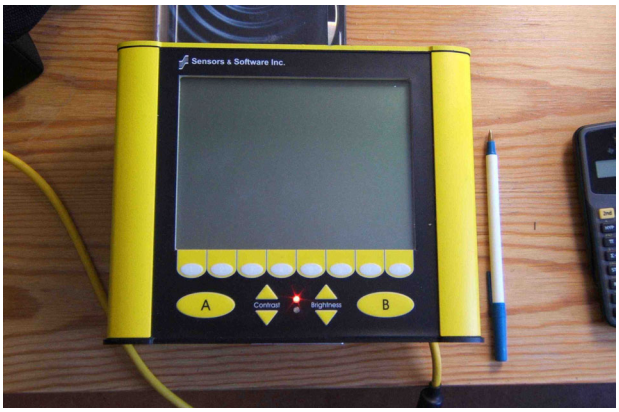

Picture 24: Close-up of radar display unit

Picture 25: Radar antenna mounted between the skids on AS350 of Airlift AS

Picture 26: Flying the radar at low level over the test site

Picture 27: Acoustics profile with sonar transducer on wetted ice surface in test trench extending from outside to inside oil skirt

Picture 28: Close-up of sonar display unit

Appendix C – Letters of Spill Permit Application and Approval

Informal English Translation from Norwegian Original

SINTEF Materials and Chemistry

Address:
NO-7465 Trondheim
NORWAY
Location:
Brattørkaia 17B, 4. etg.
Telephone:
+47 4000 3730
Fax:
+47 930 70730

Enterprise No.:
NO 948 007 029 MVA

Sysselmannen på Svalbard
Postboks 633
9171 Longyearbyen

NB! Translation of original document in Norwegian

Your ref.:	Our ref.:	Direct line:	Trondheim,
	800413/PJB	Brandvik 9095 8576	2006-02-14

Application for release of oil for research purposes

SINTEF is co-ordinating a Norwegian-American research project entitled: "New and Innovative Equipment for Remote Sensing, Detection and Tracking of oil in and under ice". SINTEF, DF Dickins Associates Ltd, USA and Boise State University, USA are the participating partners in this project. The project is financed by Norwegian and American oil companies, and also by the American government (MMS).

Aim
To develop a tool for detection and mapping/surveying of oil under sea ice when oil is accidentally spilled in or below sea ice. The trials will also be used for studying weathering of oil under ice, vertical migration of oil through the ice, and finally, in-situ burning of oil in melt-pools on ice as a method to combat oil spills in ice.

This project is a follow-up study from several earlier laboratory- and field studies without oil. For the spring of 2006 (25^{th} – 31^{st} March), we are planning the following work on the sea ice in Svea which will include releasing oil for research purposes:

Detection principle
Two different detection principles will be used to detect oil under ice. The first one is a second generation radar system tested in a basin with oil and with sea ice in Alaska without oil. In addition, ice samples will be taken for testing the concept of an "Ethane sniffer", which is a very sensitive sensor for ethane gas. The aim is to detect ethane gas from the oil through the ice. Radar and acoustic systems operated on ice, as well as radar fitted to a low flying helicopter, will be tested to map the oil (thickness and spreading).

Trials with oil under ice
In February the plan is to set out two rings with vertical skirts to keep the oil under the ice. The vertical skirt has a total depth of 150 cm and will be hanging 30-40 cm below the ice which is supposed to become 100-110 cm thick. In the end of March the skirt will be filled with 3500 litre Statfjord crude oil (average thickness 5 cm). Two similar rings will be set out to have one backup if cracks occur, or if the ice is displaced etc. Before the oil is pumped into the ring the ring will be inspected by a under water camera or a diver. In this period some equipment will be situated on the ice (small work barrack, generators etc.). This equipment will be transported with scooter/tractor and will be removed after use.

When the oil is pumped under the ice, the tests to measure thickness and spreading will be carried out along survey lines over the area. The weathering of the oil (evaporation, leakage of water soluble components) will be studied after the detection trials are terminated before Easter. The oil will slowly migrate upwards through the brine channels in the ice and is expected to surface on the ice and form so-called "melt pools" while the ice is still safe for personnel and snowmobiles in the end of May. After as short period with oil on the ice an in-situ burning experiment will be performed with oil in the melt pool. We wish to carry out an experiment with in-situ burning to calculate the ignition- and burn-efficiency of an oil spill in ice. Burning is one of the most effective combat methods for an oil spill in ice. The residue after burning will quantitatively be collected and weighted/characterised as part of the trials. This means that all the oil will be removed from the ice.

If Sysselmannen/Kystverket wishes to test ignition of oil-in-ice by helicopter and Helitorch, which is part of Kystverket's equipment in Longyearbyen, this may be included as part of the trials.

There will be some smoke emission during the actual burning trials. These will last for approximately 10-30 minutes. The burning trials will be co-ordinated with Store Norske so that eventual smoke will not hinder the air traffic in and out of Svea.

The oil will be placed on the ice outside the Crednermoraine in the bottom of the van Mijen fjord, sufficiently away from areas where Store Norske might break the ice to get access to the Svea coal export quay. The experiment site will be discretely marked with bamboo sticks, placed outside the scooter trail from Svea and Paulabreen, and will not hinder the scooter traffic. The location of the experiment site will also be announced by poster in Svea and in the field log kept by the Sysselmann.

Senior scientist Per Johan Brandvik from SINTEF Materials and Chemistry, Marine Environmental Technology will be the responsible for the release. Brandvik has extensive experience with experimental oil trials at Svalbard. He is responsible for fulfilling the conditions for release in an eventual permission from Sysselmannen. SINTEF scientists and our co-operating partners, as well as PhD and MSc students from UNIS will also participate in this project. SINTEF has entered into a long term lease agreement with Store Norske concerning taking over Polartun as a base for our project activities at Svalbard. We have for some years hired the ground floor of Barrack 29 from Store Norske for the same purpose.

A sketch of the project was presented in a meeting between you and our project manager in Longyearbyen in October 2005. Please do not hesitate to make contact if you should need further information concerning the project. This document is also sent by-email to environmental manager Rune Bergstrøm as a signed pdf-file. A more thorough project description is also enclosed this e-mail (30 pages).

Yours sincerely
SINTEF Materials and Chemistry

Tore Aunaas (sign)
Research Director

Per Johan Brandvik (sign)
Senior Scientist/Project Manager

NB! THIS IS AN UNOFFICIAL TRANSLATION OF THE ORIGINAL RELEASE PERMIT WRITTEN IN NORWEGIAN

SINTEF Materials and Chemistry
7465 Trondheim

The Governor of Svalbard
9171 Longyearbyen, Svalbard

Our contactperson:	*Our date: 16.02.2006*	*Our reference: 2006/109-2 a.552.1*
Bjarne Otnes	*Your date: 30.01.2006*	*Your reference: 800413/PJB*

SINTEF Materials and Chemistry - Permit to release oil for scientific purposes in Van Mijenfjorden

With reference to your application dated 30.01.2006 where SINTEF Materials and Chemistry apply for a permit to release 3500 litres of oil under the ice in van Mijen fjorden the last week of March 2006.

The purpose with the experiment is to develop equipment to detect and map oil under ice from an acute oil spill in or under sea ice. The experiment will also be used to study oil weathering and migration of oil in ice, and in-situ burning of oil as an oil spill contingency method.

The oil will be contained under the ice by a circular vertical skirt, sticking 30-40 cm under the ice. Migration of the oil through the brine channels will after a few weeks bring the oil to the surface, where it will be burned as a part of the field experiment. The residues will be collected and analysed.

It is the evaluation of the Governor of Svalbard that the oil will be contained and that the possibility for oil spreading in the marine environment is low. As long as the experiment is carried out as planned, air emission will be the only significant release of harmful substances to the environment.

It is the Governor of Svalbards opinion that the outcome of these experiments is important for developing efficient methods to map and combat oil spills in ice infested areas on Svalbard and in the Arctic in general. The conditions in the van Mijen fjord are good for performing such experiments in a safe manner.

Based on these evaluations is this permit given, by the Governor of Svalbard, to release and burn 3500 litres of oil in van Mijen fjorden as described in your application. The authority to give this permission is based on the Svalbard Environmental Act §57, 1b.

This permit assumes that a short report summarising the outcome of the experiment is sent to the Governors office. The Governor must also be notified, without any delay, in case of any accidents, unplanned events or changes in the field work that increase the possibility for oil to be spread in the environment.

Right to appeal
This decision taken by the Governor can be appealed within three weeks. The appeal is addressed to the Governor of Svalbard.

Regards

Rune Bergstrøm (sign)
Head of Environmental section

Bjarne Otnes (sign)
Advisor

Copy to: Store Norske Spitsbergen Kullkompani, 9170 Longyearbyen

Appendix D

NASA MODIS Images of van Mijen fjord and Svea 2006

Ice Formation and Stabilization in van Mijen fjorden 2006

March 1

March 10

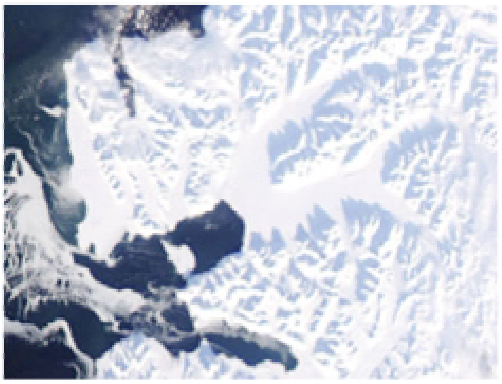

March 17

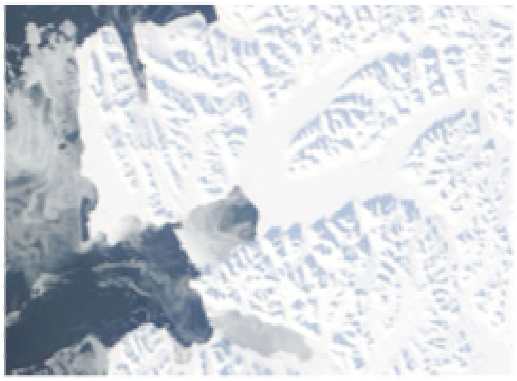

March 27

Ice Melt in van Mijen fjorden 2006

April 20

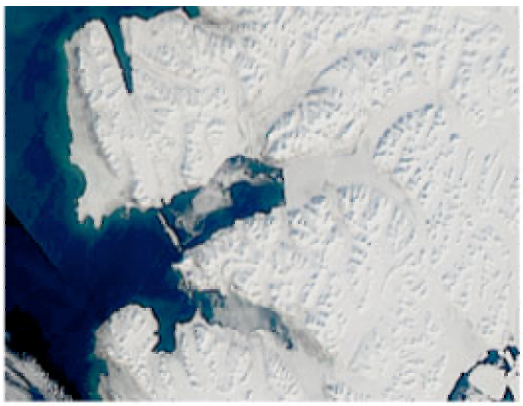

May 5

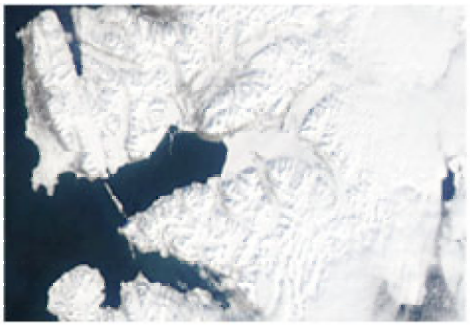

May 23

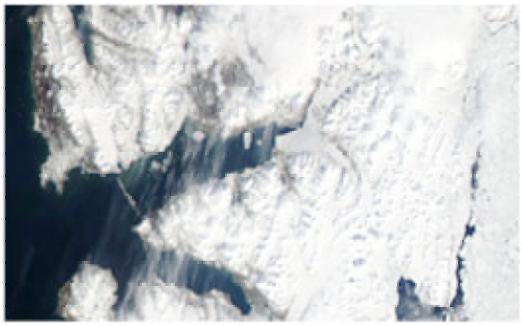

June 3

APPENDIX E

Secondary Analysis of Oil, Water, Ice Cores and Ambient Air Samples

Prepared by:
Victor Jones and Patrick Myers
Exploration Technologies Inc., Houston TX

Edited and findings summarized by: D. Dickins

Background

All petroleum spills from either man-made or natural conduits contain substantial quantities of dissolved light and gasoline range hydrocarbons. The light gases include methane, ethane, propane, iso-butane and normal-butane and the gasoline range include iso and normal pentane through xylene plus hydrocarbons. Trace levels (10's to 1000's of ppms) of these light gases are always present as dissolved phase trace hydrocarbons in all crude oils. Ethane is a vapor component at all temperatures and pressures encountered in the near-surface, making it a very mobile gas. It is also resistant to natural biodegradation and has been found to persist as an oil-related component within petroleum spills as old as 60 to 100 years in age. In addition, ethane has no biogenic sources, so that its presence provides solid evidence for the presence of a petroleum spill. A previous spill under ice at the CRREL cold basin in New Hampshire demonstrated the presence and mobility of ethane as a trace gas within an ice-water system (Dickins et al., 2005).

This technical note covers analysis conducted on a limited set of samples collected immediately before and after a larger spill under natural sea ice on Svalbard, March 27 2006. The purpose of this secondary analysis was not to duplicate the primary oil sampling and analysis conducted in Norway (findings in main report), but to provide additional understanding of the potential pathways and likelihood of detecting sufficient ethane gas components in the upper ice layers to utilize the current generation of ethane sensors represented by the Shell Global Solutions LightTouch™ system. A prototype ethane sensing system was tested directly in the previous 2004 tank tests. It was not possible within the schedule and budget to deploy the current generation sensor on Svalbard in 2006.

Whole Oil Analysis

The oil was a light paraffinic Statfjord crude that had been stored in sealed drums for a number of years. The oil was injected under the ice through a neutrally buoyant pipe inserted through an augur hole drilled at an angle just outside the skirt. A total of 3,400 litres (18 drums) was pumped under the ice. The oil was at ambient temperature at the time of injection and the air temperature was -15°C. The injection required 2 hours and ten minutes. In order to determine whether the crude contained adequate ethane, and other light hydrocarbon gases it was necessary to analyze the content of these light gases in a fresh sample. For this purpose, one oil sample was collected at the time of injection and sent to ETI for analysis of the light and gasoline range alkanes. The oil sample was analyzed by multiple GC methods in order to provide a characterization of the whole oil at the time of injection under the ice. This analysis included both the light volatile and heavier, less-volatile components, with particular focus on the concentrations of the light methane through butane vapors and the pentane plus hydrocarbons contained within the injected oil.

Quantification of the main alkane components contained within a whole oil sample requires the use of three separate gas chromatography analysis methods in order to properly analyze and quantify the very complex mix of light gas, gasoline range and heavier, non-volatile components. One method is used for the whole oil, which includes the C4 to C30 normal alkanes, a second method expands and separates the C5+ gasoline range components, and a third method is required to analyze the light C1 – C4 (methane through butane) light gas vapors. The whole oil analysis is conducted using a modification of ASTM method D-3328, a high resolution capillary gas chromatography (HRCGC) technique that is used for "fingerprinting" various types of refined and crude petroleum products. This whole oil analysis provides a "fingerprint" analyses of the C4 to C40 alkanes, that also includes a low-resolution display of the C5+ gasoline range hydrocarbons, and the aromatic BTEX (benzene, toluene, ethylbenzene, m&p-xylenes and o-xylene) hydrocarbons contained in the crude oil.

This initial, whole oil analysis was performed on a Hewlett Packard 5890 gas chromatograph equipped with a flame ionization detector (FID) with helium as a carrier gas. The column is a J&W Scientific DB-1 capillary column (0.5u, 0.5mmx30M). For free products a volume equal to 0.1 µl of oil is withdrawn from the sample bottle with a precision 1.0µl syringe. The GC run starts at an initial temperature of -12°C which then ramps at 7 degrees per minute to a maximum temperature of 350°C. A plot of the chromatogram for each sample is generated along with retention times, integrated areas and quantitated, providing concentrations for each identified component peak.

C1 – C4, C5+ Analysis

For analysis of the light C1 – C4 gases and the expanded C5+ gasoline range vapors, a saturated vapor sample is generated directly from the oil by placing 2 ml (0.06 f.oz) of the oil in a closed 125 ml (4.22 f.oz) bottle. The concentrations of the light C1 – C4 and C5+ components are then analyzed from the content of the saturated vapors in the headspace at room temperature. Analyses of the expanded C5+ (pentane through xylenes+) gasoline range hydrocarbons and BTEX (benzene, toluene, ethylbenzene, m&p-xylenes and o-xylene) aromatic hydrocarbons are completed on a Hewlett Packard

5890 gas chromatograph equipped with a flame ionization detector (FID) with helium as a carrier gas. The column is a Restek RTX-1 capillary column (0.5u, 0.5mmx30M). This analysis is also a modification of method ASTM D-3328. A volume of gas equal to 500 µl is withdrawn from the sample bottle using a gas-tight syringe and manually injected. The GC run starts at an initial temperature of 30°C which then ramps at 5 degrees per minute to a maximum temperature of 110°C. The light hydrocarbon (C1-C4) compounds are analyzed on a custom built ETI gas chromatograph equipped with a specially designed high sensitivity flame ionization detector. An 80/100 mesh alumina packed column is used for chromatographic separation; a sensitivity of 20 ppbv for methane through butanes (C1-C4) can be obtained with this instrument. The sample is flowed through the GC sample loop from the sample bottle and automatically injected onto a 3 foot alumina packed, 1/8 inch ID column. Computer controlled valves isolate the injected sample within a 2.7 cc sample injection loop. The sample is carried through the chromatographic column by purified nitrogen carrier gas. An isothermal temperature of 95°C is used for this analysis.

C1 – C4 and Ethane Analysis

The headspace light gas concentrations in the injected Stratford oil sample were analyzed in duplicate to demonstrate reproducibility. Ethane concentrations were significant, exceeding 3200 ppmv in the saturated vapor headspace in contact with the oil sample. The C1 - C4 results analyzed in duplicate from a vapor headspace oil sample in ppmv are as follows:

Component	methane	ethane	propane	iso-butane	Normal-butane
Sample 1	96	3,220	27,372	8,490	37,598
Sample 2	102	3,301	27,303	8,469	37,487

These concentrations are in the upper quartile when compared with examples of other oils previously tested at ETI's lab under identical procedures, indicating that this Stratfjord crude oil contains an adequate amount of ethane for this study. In contrast, the South Louisiana crude oil used in the previous 2004 CRREL study contained 560 ppmv methane and 5000 ppmv ethane. Propane, iso-butane and normal-butane were nearly the same at 27,000, 14,000 and 37,000 ppmv, respectively as in the South Louisiana Crude Oil used for the CRREL test.

The C5+ gasoline range components were also analyzed in duplicate. Chromatographic and tabular results are included in this Appendix for reference with the previous CRREL study as required.

Air, Water and Ice Core Sample Collection and Analysis

In order to establish background concentrations of the light C1 – C4 gases before the oil was injected into the test skirt, one air and water sample was collected, along with a full depth ice core drilled adjacent to (outside) the skirt containment. This core was divided into six 10 cm sections. After the oil was injected under the ice, one additional air sample and three post-water samples were collected, along with a second series of ice core samples. These samples were packed for shipment to the UNIS laboratory in Longyearbyen (ice structure and oil analysis), the SINTEF laboratory in Trondheim (oil and water soluble components) and to ETI's laboratory in Houston, Texas (for analysis of light and gasoline range hydrocarbons trapped in the ice, or dissolved in the water). These post-spill samples were collected to determine the impact of oil-related gas migration into the ice sheet.

Collection and handling methods are summarized here for the different sample types:

Ice cores:	Ice cores were collected with a clean core barrel (prior to any contact with gross oil). The coring team were instructed not to touch the core to avoid contact with oiled work gloves. The core was allowed to slide out of the barrel on its own to rest on the clean snow surface for collection. At that point the core was retrieved while wearing rubber gloves and laid out on a clean sheet of aluminum foil on a work bench. The core was sliced with a saw and each section then scraped with a clean knife blade all round to fit in side the opening of the plastic bell mouth sample jars.
Air Samples:	Collected by unscrewing the lid of the sample jar and holding into the prevailing wind at an elevation of approximately 1 m above the ice surface.
Water Samples:	Collected by dipping and open sample jar below the surface of the dive holes. In the case of the diver-collected sample, the sealed jar was carried beneath the surface on a wrist lanyard (rope taped to the jar) and opened to allow water ingress while approximately 20 cm below the oil layer under the ice.

Pre-spill Samples

Air

One pre-spill and one post-spill air sample were collected for analysis by GC technologies. Light C1 – C4 hydrocarbon gas chromatographs have the ability to measure ethane directly in the ambient air in the 5 to 10 ppbv range using a flow-through analysis method. Both the pre and post air samples were clean and contained only background levels of oil-related gases.

Water and Ice

One pre-spill water sample was collected by diver at a hole in the skirt, and one pre-spill ice core sample was taken at Reference point 3 (REF3) outside the test skirt. The pre-spill ice core collected at REF3 was divided into six sections that

are referred to as PreCore at REF3 location: Top 10 cm, 10-20 cm, 20-30 cm, 30-40 cm, 40-50 cm, and 50-60 cm. The ice core samples were collected in 1-liter containers and kept frozen until transported to ETI for analysis (melted enroute). These water and ice core samples were shipped to ETI's lab for analysis of light C1 – C4 and C5+ hydrocarbons.

All ice core samples were allowed to come to room temperature before analysis, and then analyzed by the flow-through method described above in the section on whole oil analysis. Detection limits for this flow through analysis are in the 5 to 10 ppbv (0.005 to 0.010 ppmv) range, with each ice core sample being run in triplicate in order to define the variance between samples. The water samples were analyzed with a slightly different protocol than the air or ice core samples because they were filled one liter water bottle samples containing only a minor headspace volume. These samples were analyzed by injecting a 1.0 cc sample from the headspace volume into the GC. Laboratory detection limits for these water headspace samples is ~30 ppb.

Results showed a small quantity of methane and ethylene in the pre-spill water sample and very low concentrations of all components in the headspace analysis of all pre-spill ice core samples. Ethane was less than 0.020 ppm and methane levels are typical of ambient air.

Post-Spill Samples

A second set of post-spill ice cores and water samples were taken on March 29 two days after the oil release. These post-spill samples included three water samples (two from the dive hole surface layer and one collected by diver beneath the oil), a second full-length core at REF3 outside of the skirt (same location as the pre-spill core), and two 20 cm long upper layer post-spill ice cores inside the oiled test area at locations 2 and 3. These cores were limited to 20 cm owing to avoid any possibility of exposing gross oil on the surface prematurely and affecting the primary SINTEF fate and behavior study.

Ice Cores

The post-spill ice cores were collected both inside and outside the skirted area in an effort to detect the presence of light C1-C4 hydrocarbons in the internal ice structure that could possibly be related to the presence of oil under the ice. Ideally, cores within the skirted area would be drilled down to within 10-20 cm of the oil layer but this was not possible, given the risk of contaminating the site. The decision not to take any cores close to full depth within the oiled area was proven to be correct by the discovery that gross oil had migrated to within 16 cm of the surface in one of the 20 cm cores.

The three post-spill ice core samples are referred to by their locations, as REF3 (outside), and Core 2 and Core 3 (inside). Results show that fairly significant light hydrocarbon (h.c.) concentrations were observed within two out of the three post-spill ice cores, whereas the pre-spill ice core was clean. Core 2 (no visible

oil during processing on site) was only minimally impacted by a small amount of normal-butane in the deeper 10-20 cm section.

A much larger concentration of ethane, propane, iso and normal-butane was found in both core sections of core 3, which was located directly over the spilled oil. The shallower core section from 0-15 cm was noted as having no visible oil and the deeper core section from 15-23 cm was noted as containing visible oil in the brine channels. The light hydrocarbon data confirms these observations. Ethylene and propylene, which are not oil related components, did not change from the top to the bottom of any of these core samples. It is significant to note that propane and butanes demonstrated a similar increase in concentration with depth as ethane, and even anomalous methane was found in the bottom section of core 3. A lack of olefins (ethylene and propylene), and the presence of the C3 and C4 associated gases confirms that all of these measured gases (including ethane) as oil-related hydrocarbons. The positive indication of light hydrocarbon components in the visibly clean top section of this core points to the potential migration of these gases from the oiled brine channels immediately below but these results could also be related to unavoidable contamination in drilling, extracting and processing the core.

The post-spill full depth ice core taken just outside the oil skirt at REF3 was also impacted within four of the six core sections; namely impact was noted within core sections from samples at depths of 10-20 cm (butane only), 20-30 cm (ethane, propane, butane), and within the bottom two core sections at 40-50 cm and bottom 2.5 cm (propane and butane). In this core, the bottom section was observed to contain fine droplets of visible oil in the soft skeletal layer (ice/water interface). The propane and butanes clearly show the increased impact on the bottom two sections of core, with the bottom section containing about 10 times as much propane and butanes as the 40-50 cm core section directly above it (not surprising given the presence of visible oil). Interestingly, only the core section from 20-30 cm exhibits any ethane contamination, and in fact, both the ethane and propane concentrations are different with respect to the butanes within this one core section as compared to the bottom two sections.

The general presence of propane and butanes without ethane throughout the post-spill ice core from REF3 might indicate the presence of contamination from handling of the two bottom core sections (one with visible gross oil). Surface oil contamination that has volatilized somewhat might be expected to lose ethane preferentially to propane and butanes. Unfortunately, it is not possible to conclusively identify the ethane in the 20-30 cm ice section as migrated oil-related gases.

Post-Spill Water Samples
Three post-spill water samples were collected by divers from holes drilled in the ice sheet. One of the post-spill water samples taken from the dive-hole was clean. The other two post-spill water samples (one from Dive hole 1 and the other from a diver 20 cm beneath the oil) are definitely impacted by oil-related light gases, with ethane and propane showing a clear dominance. The sample from the divehole could have been contaminated by a surface sheen left from cutting and clearing the ice with a chainsaw to remove the overnight growth. The submerged sample indicates the potential migration of oil-related gases into the water.

Conclusions

Results from the earlier 2004 experiment under 35 cm sea ice in a cold basin showed that measurable, but very low levels of ethane flux were being transmitted through the ice above the oiled areas. The timing of the flux measurements in that program ranged from 2 to 13 days after the oil was spilled. Ice cores analyzed from the basin ice demonstrated that light gases such as ethane had penetrated nearly to the surface within two weeks. The 2004 study concluded that the detection of ethane migrating through solid ice above a trapped oil layer was feasible, given sufficient time following the spill. However, it was not possible to estimate how much time would be needed for ethane to migrate through a meter or more of natural sea ice, or whether the flux levels in a natural field setting would be sufficient to permit reliable detection.

Sampling in 2006 was limited to immediately pre and post spill (within 48 hours). A warming trend after the spill led to early melt of the already thin ice cover and encouraged gross oil migration through ice, precluding further sampling for light hydrocarbon gas components. The limited dataset obtained from the available samples showed that the light C1 - C4 gases may migrate rapidly into the adjacent water in contact with the oil. However, evidence of significant vertical migration of these gases through the ice sheet is not conclusive from the post-spill core samples.

Elevated levels of a range of light gases (including ethane) were found immediately above visible oil-filled brine channels in one short core taken within the test skirt. There was no evidence of gas migration in the other short core (top 20 cm) where no oil migration was visible. The post-spill 60 cm core taken immediately outside the test skirt did show elevated levels of only butane, and propane in the bottom two sections above visible fine oil droplets. Elevated levels of ethane, propane and butane were measured in the section from 20-30 cm depth (from the surface), but it was not possible in that case to conclusively identify the ethane as related to the spilled oil. Additional reference samples may have helped rule out the possibility of sample contamination, keeping in mind that maintaining a pristine environment in a field setting with mechanical equipment is extremely difficult.

Fundamental questions remain to be answered or addressed in future experiments in order to develop any overall conclusions about the practical application of ethane or other gas sensors in Arctic spill response:

- How long will the oil contain adequate levels of light C1 – C4 and C5+ hydrocarbon gases after being spilled and trapped under the ice to enable subsequent detection of ethane flux at the surface or from an airborne platform?
- Do ethane and other light gas components migrate reliably through a solid ice sheet within a short enough period of time to provide a practical marker for detection in the case of an accidental spill where time could be critical in mounting a response?